patch area. This was evident irrespective of whether staining was with CaN, GFAP, or Nissl stain.

Cell Type–Specific Loss of Striatal Neurons

Large cholinergic interneurons account for only 1 to 2 % of striatal neuronal populations[25]; however, they exert a pivotal role in the striatal functions.[26] To determine their susceptibility to neurodegeneration in XDP, we performed immunostaining with antibody to ChAT, a specific marker for cholinergic neurons. Microscopically, there was no apparent difference between normal controls (Fig 6A, C) and XDP-D patients (Fig 6B, D) in the distributional profile of striatal $ChAT^+$ neurons. Cell density analysis (Fig 6E) disclosed that the number of $ChAT^+$ cells/mm^2 in the neostriatum of normal controls was 4.4 ± 1.6 ($n = 20$), and that of XDP patients was 4.9 ± 1.8 ($n = 20$). Thus, large cholinergic neurons were spared in the striatum of patients with XDP-D. This finding indicates that there is a cell type–specific difference in vulnerability to neurodegeneration in the XDP neostriatum, with the preferential loss of medium spiny neurons and sparing of cholinergic neurons. Similar cell type–specific loss of striatal neurons has also been reported in other pathological conditions such as Huntington's disease (HD)[27–33] and cerebral ischemia.[31,32,34,35]

Change in the Striatopallidal Projections

The matrix compartment includes two different projecting cell populations.[11–15] The indirect pathway neurons project to the external segment of the globus pallidus (GPe), the direct pathway neurons project to its internal segment (GPi), and the substantia nigra pars reticulata (SNr). In normal controls, strong CaN labeling of the striatopallidal projections was found in both the GPe and GPi (Fig 7A), where CaN^+ fiber plexuses were abundant (Fig 7B, C). Their configuration was that of the so called "woolly fibers"[36] and consisted of unstained dendrites of the pallidal neurons densely coated with the labeled axon terminals of striatal projection neurons.[37] In XDP-D patients (see Fig 7D), CaN labeling was diminished in both the GPe and GPi, where the number of CaN^+ axon plexuses was reduced and woolly fibers were occasionally found (see Fig 7E, F). There was no apparent difference between the GPe and GPi in the degree of sparing of CaN^+ fibers. In XDP-P patients (see Fig 7G), there was a marked loss of CaN labeling in both the GPe and GPi where CaN^+ axon plexuses were severely depleted and no woolly fibers were identified (Fig 7H, I), reflecting a severe depletion of striatal projecting neurons.

Change in the Striatonigral Projections

Normally, efferent projections from the striosomes and matrix compartment differentially innervate the substantia nigra (SN)[12,24]: striosomal cells provide inputs to the location of dopaminergic cells in the substantia nigra pars compacta (SNc) and islands of dopaminergic

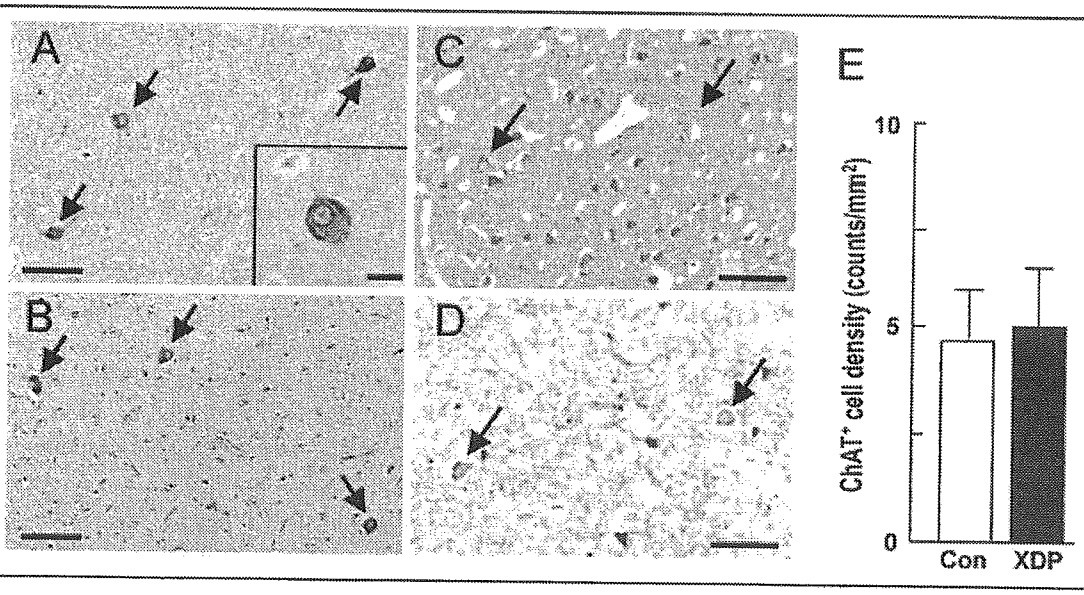

Fig 6. Sparing of $ChAT^+$ neurons in the X-linked recessive dystonia parkinsonism with dystonia (XDP-D) neostriatum. (A, B) ChAT immunostaining of the neostriatum from a normal control (A) and an XDP-D patient (B). $ChAT^+$ neurons are indicated by arrows. *The* inset *in (A) is a high-power image of $ChAT^+$ neuron. (C, D) Double immunostaining for ChAT (brown) and CaN (blue). In a normal control (C), $ChAT^+$ neurons* (arrows) *are surrounded by many neurons positive for CaN in the neostriatum. However, in an XDP-D patient (D), spared $ChAT^+$ neurons are frequently found in the neostriatal area poor in CaN^+ neurons (ie, the interpatch area). (E) The numbers of $ChAT^+$ cells/mm^2 in the neostriatum from normal controls (Con) and XDP patients (XDP). There is no apparent difference between controls* (unfilled column) *and XDP patients* (filled column) *in the cell density of $ChAT^+$ neurons in the neostriatum. Scale bar (A–D) = 100 μm: Scale bar* (inset *in A) = 20 μm.*

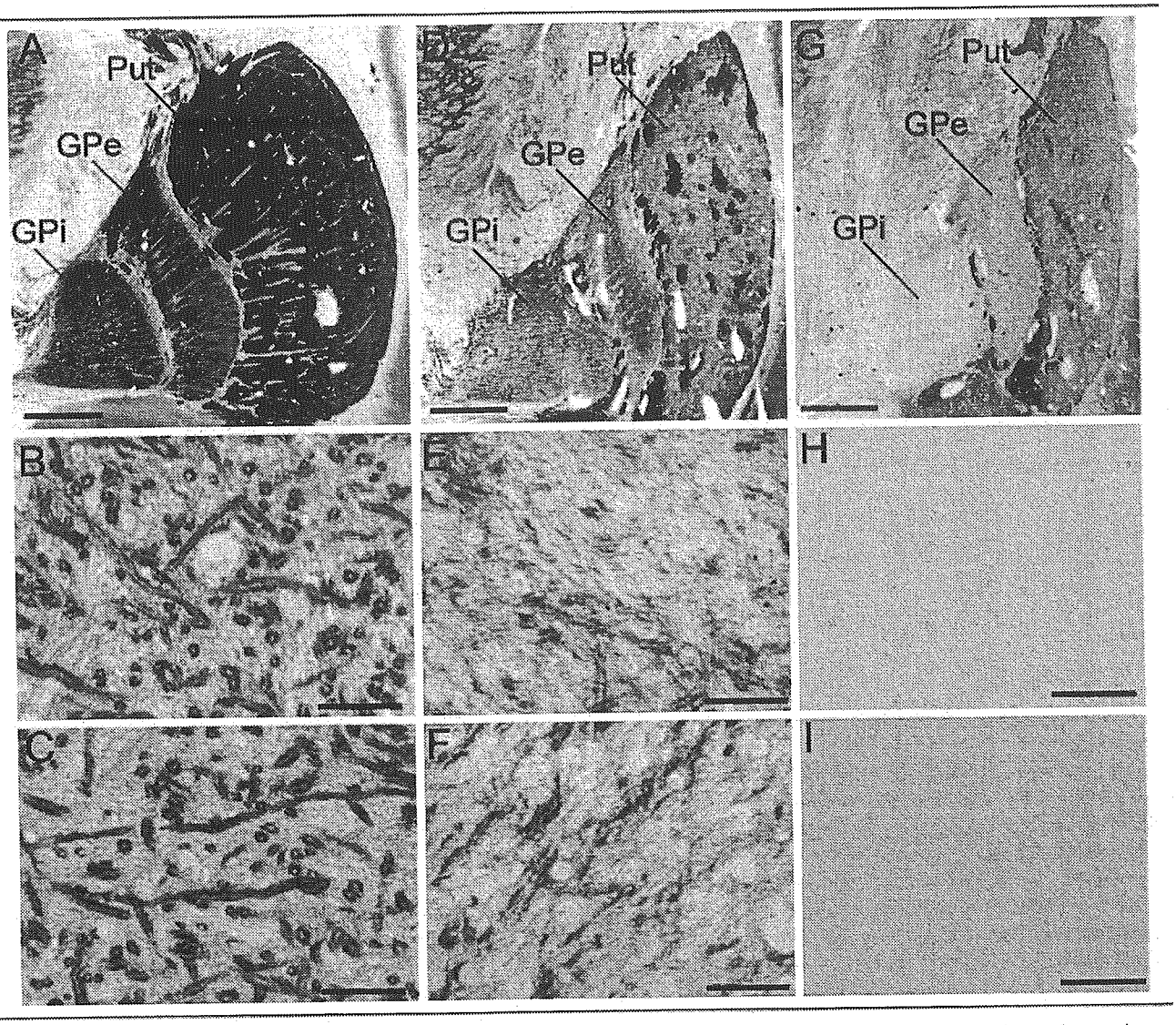

Fig 7. Striatopallidal projections visualized by calcineurin (CaN) immunostaining. CaN immunostaining of the lenticular nucleus from a normal control (A–C), an X-linked recessive dystonia parkinsonism with dystonia (XDP-D) patient (D–F), and an XDP with parkinsonism (XDP-P) patient (G–I). (A–C) Normally, strong CaN labeling of the striatal projection fibers is found in both the GPe and GPi (A). Microscopically, CaN^+ fiber plexuses are abundant in the GPe (B) and GPi (C). They are reminiscent of woolly fibers consisting of the unstained dendrites of the pallidal neurons densely coated with the labeled axon terminals of striatal projection neurons. (D–F) In an XDP-D patient, CaN labeling is significantly diminished in the GPe and GPi (D). Microscopically, the number of CaN^+ fiber plexuses is reduced and woolly fibers are occasionally found in the GPe (E) and GPi (F). Note that there is no apparent difference between the GPe and GPi in the degree of remaining CaN labeling. (G–I) In an XDP-P patient, there is a severe depletion of the CaN labeling of striatal projections in both the GPe and GPi (G). Microscopically, CaN^+ fibers are severely depleted in both the GPe (H) and GPi (I) and no woolly fibers are identified. Scale bar (A, D, G) = 2.5mm: Scale bar (B, C, E, F, H, I) = 50 μm.

cells in the SNr, whereas matrix cells provide inputs to the location of nondopaminergic neurons in the SNr. In normal controls, CaN^+ afferent fibers of the striatonigral pathway were diffusely distributed in almost the entire SN (Fig 8A). In the SN of XDP-D patients, there was a significant diminution of the CaN^+ fibers and the remaining CaN^+ fibers were unevenly and compartmentally distributed (see Fig 8B). Their distributional profile was almost identical to that of the remaining $Calb^+$ fibers of the matrix-based striatonigral projections in the SNr (see Fig 8C). We encountered no apparent loss of TH^+ dopaminergic neurons in the SN of XDP patients, as reported previously.[4,5,8,9] Analysis of serially adjacent sections stained for TH (see Fig 8D) and CaN (see Fig 8E) showed that the remaining CaN^+ fibers were substantially found in the SNr but not the SNc (see Fig 8F). These findings indicate a preferential loss of the striosomal pathway and the rel-

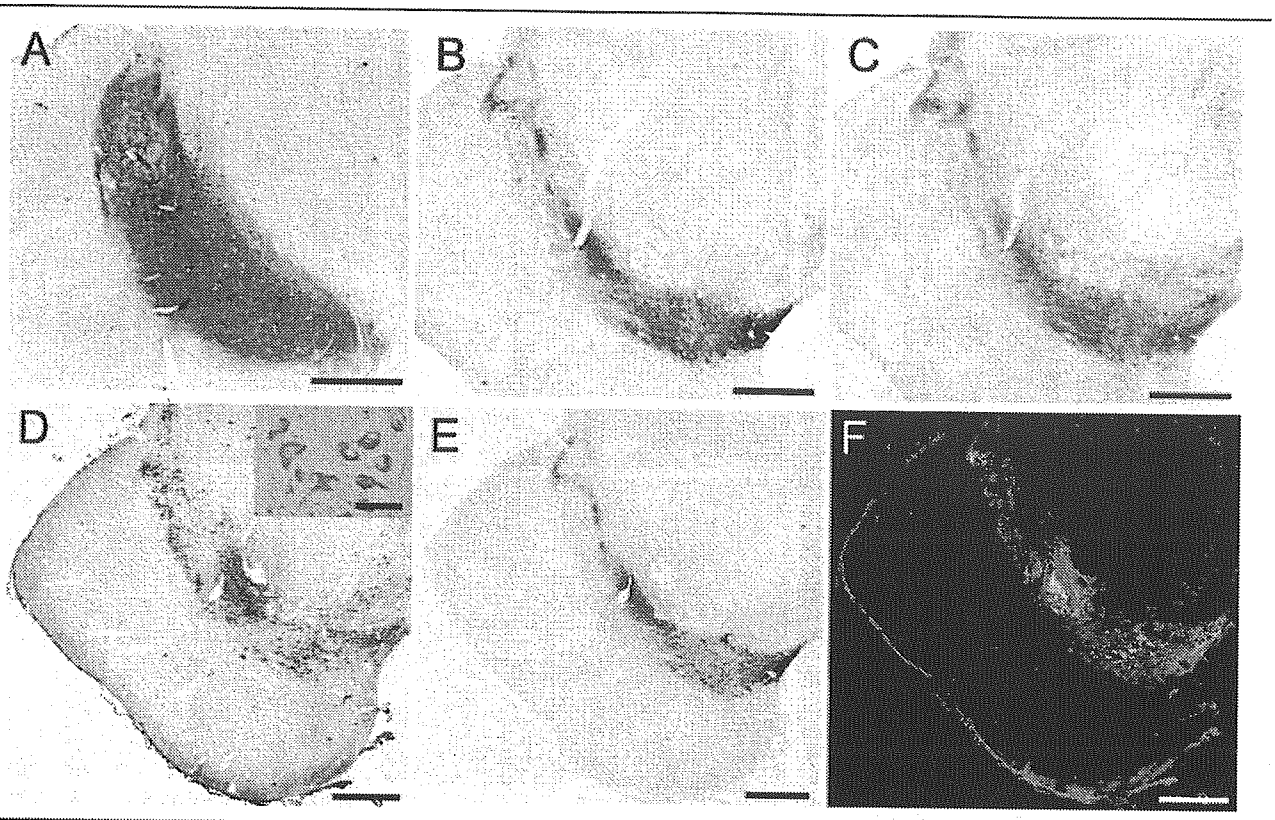

Fig 8. Immunohistochemical findings on the substantia nigra (SN). (A) Calcineurin (CaN) staining of the SN from a normal control. Strong CaN labeling is almost diffusely distributed in the entire SN. (B, C) Serially adjacent midbrain sections stained for CaN (B) and Calb (C) from a patient with X-linked recessive dystonia parkinsonism with dystonia (XDP-D). CaN labeling is significantly diminished in the SN, where the remaining CaN labeling of the striatonigral projections is unevenly and compartmentally distributed (B). Normally, $Calb^+$ fibers of the striatonigral pathway originating from the matrix compartment are densely distributed in the substantia nigra pars reticulata (SNr), although calbindin is also localized in a subpopulation of substantia nigra pars compacta (SNc) neurons and in a large number of ventral tegmental area neurons.[24] The distribution profile of the remaining CaN labeling (B) is almost identical to that of the remaining $Calb^+$ fibers of the matrix-based striatonigral projections (C) in the SNr. (D–F) Serially adjacent midbrain sections stained for tyrosine hydroxylase (TH) (D) and CaN (E) from an XDP-D patient. TH and CaN immunoreactivity was digitally changed to green and red, respectively, and a merged image is shown in F. The inset *in D is a high-power image of TH^+ neurons. TH^+ dopaminergic neurons are normally spared in the SNc (D). In primates, the precise differentiation between the SNr and SNc is difficult because of the interdigitation of the dopaminergic neurons of the SNc with the nondopaminergic neurons of the SNr.[42] We used the presence of TH^+ neurons to define the location of the SNc. Note that in the SN, the distribution of CaN staining (E) is almost complementary to that of TH staining (D); this is also evident in (F). Scale bar (A–F) = 2.5mm: Scale bar (the* inset *in D) = 50 μm.*

ative sparing of the matrix-based pathway in XDP-D. In XDP-P, there was a marked reduction of CaN^+ fibers in the SN (data not shown), as well as the GPe and GPi.

Discussion

Our results show that there is a compartmental and cell type–specific loss of neurons in the neostriatum of XDP patients. Of great interest is that in the XDP-D neostriatum, the matrix compartment is relatively spared, whereas the striosome compartment is severely depleted. This coincides with the preferential loss of the striosomal pathway and the relative sparing of the matrix-based pathway in the SN of XDP-D patients. These findings indicate that in XDP-D there is a disproportionate involvement of the striatal compartments leading to an imbalance in the activity between the striosomal and matrix-based pathways. As suggested in other pathological conditions such as cerebral hypoxia-ischemia[38] and HD,[39] the preferential loss of the striosome compartment may cause the abnormalities of motor control by the basal ganglia, resulting in the occurrence of neurological symptoms in patients with XDP.

The onset of XDP is in adulthood, by the end of the third or the early part of the fourth decade.[4,5] It manifests predominantly as dystonia that spreads and becomes generalized over 2 to 5 years, reaches a plateau by the 10th year, and then becomes less severe or is replaced by parkinsonism by the 15th year of illness.[4,5]

In view of the three-pathway basal ganglia model (Fig 9), we suggest that at the earlier stage when dystonia manifests predominantly (dystonia stage), severe loss of striosomal GABAergic projection neurons that form the striosomal pathway leads to disinhibition of nigral dopaminergic neurons, thereby increasing the action of striatal dopamine on the remaining matrix neurons. This then results in the hyperkinetic disorder dystonia and may comprise a vicious cycle that accelerates striatal neurodegeneration, through dopamine-mediated toxicity to striatal neurons.[40,41] In addition, eventual loss of the indirect pathway neurons also may underlie the occurrence of dystonia in XDP, as suggested for the genesis of chorea in HD.[42,43] At the later stage when dystonia is less severe and is replaced by parkinsonism (parkinsonism stage), the greater involvement of the matrix compartment leads to a severe and critical reduction of matrix-based projections and thus to the development of so-called "extranigral form" of parkinsonism. This condition has also been suggested in the late stage of HD[33,42–44] and a form of multiple system atrophy (ie, striatonigral degeneration).[18,45] Positron emission tomography findings[46] suggested that parkinsonism in XDP might be secondary to extranigral factors.

Among the basal ganglia disorders, XDP shares common features with HD, another adult-onset genetic movement disorder,[47–49] for example, the progression of neurological signs and striatal pathology that includes the preferential loss of medium spiny projection neurons and sparing of large cholinergic interneurons. Despite hypotheses to explain the occurrence of hyperkinetic symptoms (eg, chorea) in HD, debate continues on this intriguing issue.[14,39,42,43,50] This study shows no apparent difference between the GPe and GPi in the degree of sparing of striatopallidal projection fibers in XDP. This suggests that in XDP there is no differential loss of indirect and direct pathway neurons. Alternatively, the direct and indirect pathway model[13,14] may not adequately explain the functional anatomy of the basal ganglia for the manifestation of dystonia in XDP. These data suggest that the dystonia in XDP may result from an imbalance in the activity between the striosomal and matrix-based pathways, and that XDP, particularly at the earlier stage, can be a human disease model to study the implication of reduced activity of the striosomal pathway in the genesis of dystonia. As shown here for XDP, the three-pathway basal ganglia model[15] may give new insights into the functional anatomy of basal ganglia disorders and may lead to rational therapeutics. For instance, we posit that the use of dopamine depleters such as reserpine

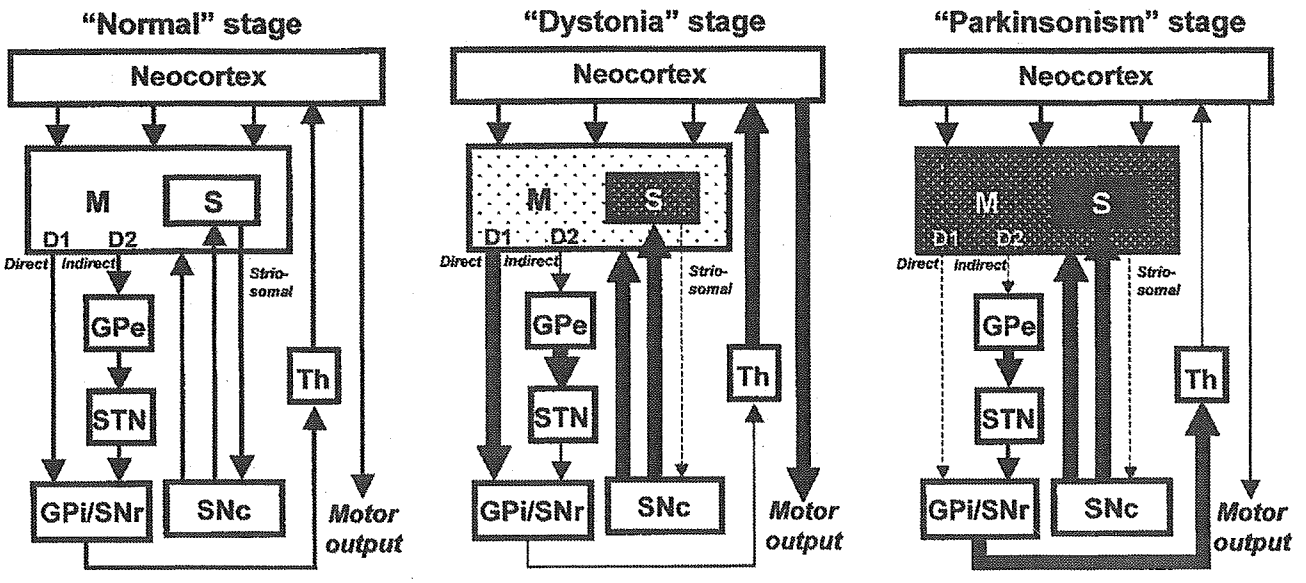

Fig 9. Hypothesized diagram of neurological progression and three-pathway basal ganglia model in X-linked recessive dystonia parkinsonism (XDP). At the earlier stage when dystonia predominantly manifests ("dystonia" stage), severe loss of the striosomal GABAergic projection neurons that form the striosomal pathway may lead to disinhibition of the nigral dopaminergic neurons, resulting in a striatal increase of dopamine action on the remaining matrix neurons and the subsequent manifestation of the hyperkinetic disorder dystonia. In addition, eventual loss of the indirect pathway neurons also may underlie the occurrence of dystonia. At the later stage when dystonia is less severe and is replaced by parkinsonism ("parkinsonism" stage), the more comprehensive involvement of the matrix compartment associated with a severe and critical reduction of matrix-based projections may result in the development of the "extranigral form" of parkinsonism. M = matrix compartment; S = striosomal compartment; GPi = internal segment of the globus pallidus; GPe = external segment of the globus pallidus; STN = subthalamic nucleus; SNr = substantia nigra pars reticulata; SNc = substantia nigra pars compacta; Th = thalamus.

may be helpful in XDP-D patients. Studies are under way in our laboratories to elucidate the pathogenic mechanisms of neuronal degeneration that is of adult onset and that occurs compartmentally and cell type specifically in the neostriatum of XDP patients.

This work was supported by grants from the Ministry of Education, Culture, Sports, Science and Technology of Japan, (grant-in-aid for Scientific Research, 15500240, S.G., Center of Excellence, 16101J-1, R.K.) from the Ministry of Education, Culture, Sports, Science and Technology of Japan.

We are grateful to M. Obata for her excellent technical assistance. We also thank R. B. Icasiano and J. Arancillo of the Roxas City Health Office, C. J. Demaisip of Iloilo City, R. Lo of the Pathology Division, Allied Medical Department of the Philippine Children's Medical Center (PCMC), R. Teleg (research fellow) and O. Peralta (research assistant) of Child Neuroscience Division, Clinical Department of PCMC for the acquisition, storage and preliminary transport of autopsied brains of XDP patients, and J. Lecciones of the Institutional Planning and Development Office of PCMC for his comments and suggestions.

References

1. Fahn S, Bressman SB, Marsden CD. Classification of dystonia. Adv Neurol 1998;78:1–10.
2. Lee LV, Pascasio FM, Fuentes FD, Viterbo GH. Torsion dystonia in Panay, Philippines. Adv Neurol 1976;14:137–151.
3. Lee LV, Kupke KG, Caballar-Gonzaga F, et al. The phenotype of the X-linked dystonia-parkinsonism syndrome: an assessment of 42 cases in the Philippines. Medicine 1991;70:179–187.
4. Lee LV, Munoz EL, Tan KT, Reyes MT. Sex kinked recessive dystonia parkinsonism of Panay, Philippines (XDP). Mol Pathol 2001;54:362–368.
5. Lee LV, Maranon E, Demaisip C, et al. The natural history of sex-linked recessive dystonia parkinsonism of Panay, Philippines (XDP). Parkinsonism Relat Disord 2002;9:29–38.
6. de Carvalho, Aguiar PM, Ozelius LJ. Classification and genetics of dystonia. Lancet Neurol 2002;1:316–325.
7. Haberhausen G, Schmitt I, Kohler A, et al. Assignment of the dystonia-parkinsonism syndrome locus, DYT3, to a small region within a 1.8-Mb YAC contig of Xq13.1. Am J Hum Genet 1995;57:644–650.
8. Altrocchi PH, Forno LS. Spontaneous oral-facial dyskinesias: neuropathology of a case. Neurology 1983;33:802–805.
9. Waters CH, Faust PL, Powers J, et al. Neuropathology of lubag (X-linked dystonia parkinsonism). Mov Disord 1993;8:387–390.
10. Singleton AS, Hague S, Hernandez D. X-linked recessive dystonia parkinsonism (XDP; Lubag; DYT3). Adv Neurol 2004; 94:139–142.
11. Graybiel AM. Neurotransmitters and neuromodulators in the basal ganglia. Trends Neurosci 1990;13:244–254.
12. Gerfen CR. The neostriatal mosaic: multiple levels of compartmental organization in the basal ganglia. Annu Rev Neurosci 1992;15:285–320.
13. DeLong MR. Primate models of movement disorders of basal ganglia origin. Trends Neurosci 1990;13:281–289.
14. Albin RL, Young AB, Penny JB. The functional anatomy of disorders of the basal ganglia. Trends Neurosci 1995;18:63–65.
15. Graybiel AM, Canales JJ, Capper-Loup C. Levodopa-induced dyskinesias and dopamine-dependent stereotypies: a new hypothesis. Trends Neurosci 2000;23(suppl):S71–S77.
16. Shi SR, Key ME, Kalra KL. Antigen retrieval in formalin-fixed, paraffin-embedded tissues: an enhancement method for immunohistochemical staining based on microwave oven heating of tissue sections. J Histochem Cytochem 1991;39:741–748.
17. Goto S, Hirano A, Rojas-Corona RR. An immunohistochemical investigation of the human neostriatum in Huntington's disease. Ann Neurol 1989;25:298–304.
18. Goto S, Hirano A, Matsumoto S. Subdivisional involvement of nigro-striatal loop in idiopathic Parkinson's disease and striatonigral degeneration. Ann Neurol 1989;26:766–770.
19. Goto S, Hirano A, Matsumoto S. Immunohistochemical study of the striatal efferents and nigral dopaminergic neurons in parkinsonism-dementia complex on Guam in comparison with those in Parkinson's and Alzheimer's diseases. Ann Neurol 1990;27:520–527.
20. Goto S, Nagahiro S, Ushio Y, Hofer W. A simple enhancement method for silver-gold intensified diaminobenzidine reaction in the immunoperoxidase technique. J Histochem Cytochem 1992;40:1423–1425.
21. Goto S, Hirano A. Catecholaminergic neurons in the parabrachial nucleus of normal individuals and patients with idiopathic Parkinson's disease. Ann Neurol 1991;30:192–196.
22. Hamasaki T, Goto S, Nishikawa S, Ushio Y. A role of netrin-1 in the formation of the subcortical structure striatum: repulsive action on the migration of late-born striatal neurons. J Neurosci 2001;21:4272–4280.
23. Smith Y, Bevan MD, Shink E, Bolam JP. Microcircuitry of the direct and indirect pathways of the basal ganglia. Neuroscience 1998;86:353–387.
24. Gerfen CR, Baimbridge KG, Miller JJ. The neostriatal mosaic: compartmental distribution of calcium-binding protein and parvalbumin in the basal ganglia of the rat and monkey. Proc Natl Acad Sci USA 1985;82:8780–8784.
25. Phelps PE, Houser CR, Vaughn JE. Immunocytochemical localization of choline acetyltransferase within the rat neostriatum: a correlated light and electron microscopic study of cholinergic neurons and synapses. J Comp Neurol 1985;238:286–307.
26. Kaneko S, Hikida T, Watanabe D, et al. Synaptic integration mediated by striatal cholinergic interneurons in basal ganglia function. Science 2000;289:633–637.
27. Ferrante RJ, Kowall NW, Beal MF, et al. Selective sparing of a class of striatal neurons in Huntington's disease. Science 1985; 230:561–563.
28. Beal MF, Kowall NW, Ellison DW, et al. Replication of the neurochemical characteristics of Huntington's disease by quinolinic acid. Nature 1986;321:168–172.
29. Ferrante RJ, Beal MF, Kowall NW, et al. Sparing of acetylcholinesterase-containing striatal neurons in Huntington's disease. Brain Res 1987;411:162–166.
30. Kowall NW, Ferrante RJ, Martin JB, et al. Patterns of cell loss in Huntington's disease. Trends Neurosci 1987;10:24–29.
31. Calabresi P, Centonze D, Pisani A, et al. Striatal spiny neurons and cholinergic interneurons express differential inonotropic glutamatergic responses and vulnerability: implications for ischemia and Huntington's disease. Ann Neurol 1998;43:586–597.
32. Calabresi P, Centonze D, Pisani A, Bernardi G. Metabotropic glutamate receptors and cell-type-specific vulnerability in the striatum: implication for ischemia and Huntington's disease. Exp Neurol 1999;158:97–108.
33. Cicchetti F, Prensa L, Wu Y, Parent A. Chemical anatomy of striatal interneurons in normal individuals and in patients with Huntington's disease. Brain Res Rev 2000;34:80–101.
34. Francis A, Pulsinelli WA. The response of GABAergic and cholinergic neurons to transient cerebral ischemia. Brain Res 1982; 243:271–278.

35. Chesselet M-F, Gonzales C, Lin CS, et al. Ischemic damage in the striatum of adult gerbil: relative sparing of somatostatinergic and cholinergic interneurons contrasts with loss of efferent neurons. Exp Neurol 1990;110:209–218.
36. Haber SN, Nauta WJH. Ramification of the globus pallidus in the rat as indicated by patterns of immunohistochemistry. Neuroscience 1983;9:245–260.
37. Goto S, Hirano A, Rojas-Corona RR. Immunohistochemical visualization of afferent nerve terminals in human globus pallidus and its alteration in neostriatal neurodegenerative disorders. Acta Neuropathol 1989;78:543–550.
38. Burke RE, Baimbridge KG. Relative loss of striatal striosome compartment, defined by calbindin-D28k immunostaining, following developmental hypoxic-ischemic injury. Neuroscience 1993;56:305–315.
39. Hedreen JC, Folstein E. Early loss of neostriatal striosome neurons in Huntington's disease. J Neuropathol Exp Neurol 1995; 54:105–120.
40. Jakel RJ, Maragos WF. Neuronal cell death in Huntington's disease: a potential role for dopamine. Trends Neurosci 2000; 23:239–245.
41. Cyr M, Beaulieu J-M, Laakso A, et al. Sustained elevation of extracellular dopamine causes motor dysfunction and selective degeneration of striatal GABAergic neurons. Proc Natl Acad Sci USA 2003;100:11035–11040.
42. Reiner A, Albin RL, Anderson KD, et al. Differential loss of striatal projection neurons in Huntington's disease. Proc Natl Acad Sci USA 1988;85:5733–5737.
43. Albin RL, Reiner A, Anderson KD, et al. Striatal and nigral neuron subpopulations in rigid Huntington's disease: implications for the functional anatomy of chorea and rigidity-akinesia. Ann Neurol 1990;27:357–365.
44. Young AB, Shoulson L, Penny JB, et al. Huntington's disease in Venezuela: neurologic features and functional decline. Neurology 1986;36:244–249.
45. Goto S, Matsumoto S, Ushio Y, Hirano A. Subregional loss of putaminal efferents to the basal ganglia output nuclei may cause parkinsonism in striatonigral degeneration. Neurology 1996;47: 1032–1036.
46. Eidelberg D, Takikawa S, Wilhelmsen K, et al. Positron emission tomographic findings in Filipino X-linked dystonia-parkinsonism. Ann Neurol 1993;34:185–191.
47. Albin RL, Tagle DA. Genetics and molecular biology of Huntington's disease. Trends Neurosci 1995;18:11–14.
48. Bossy-Wetzel E, Schwarzenbacher R, Lipton SA. Molecular pathways to neurodegeneration. Nat Med 2004;10(suppl):S2–S9.
49. Li SH, Li XJ. Huntingtin-protein interactions and the pathogenesis of Huntington's disease. Trends Genet 2004;20:146–154.
50. Seto-Ohshima A, Emson PC, Lawson E, et al. Loss of matrix calcium-binding protein-containing neurons in Huntington's disease. Lancet 1988;1:1252–1255.

Herpes Simplex Encephalitis Presenting with Bilateral Hippocampal Lesions on Magnetic Resonance Imaging, Simultaneously Complicated by Small Cell Lung Carcinoma

Ryo HIRAI, Mitsuyoshi AYABE, Hiroshi SHOJI, Masahide KAJI*, Takashi ICHIYAMA** and Koichiro SAKAI***

Abstract

We report a 75-year-old man who developed herpes simplex encephalitis (HSE), presenting with bilateral hippocampal lesions on magnetic resonance imaging, and this case was simultaneously complicated by small cell lung carcinoma. We identified a new anti-neuronal antibody in the cerebrospinal fluid of this patient. Our findings suggest that HSE and paraneoplastic limbic encephalitis (PLE) can overlap, and we discuss the relationships of HSE, PLE, and related disorders.
(Internal Medicine 44: 1006–1008, 2005)

Key words: herpes simplex encephalitis, paraneoplastic limbic encephalitis, non-herpetic acute limbic encephalitis

Introduction

Herpes simplex encephalitis (HSE) is the most common acute encephalitis. It selectively affects the temporal lobes and frontal lobes including the limbic system (1–3). Paraneoplastic limbic encephalitis (PLE) reveals subacute dementia with magnetic resonance imaging (MRI) abnormalities in the medial temporal lobes, and it is associated with lung or testicular cancer (4, 5). In the course of a survey of HSE in the Kyushu and Okinawa regions of Japan, non-herpetic acute limbic encephalitis (non-herpetic ALE) was found (6–8). Presently, the pathogenesis of these limbic forms of encephalitis, or what forms the spectrum of HSE, PLE, and related limbic encephalitis, is controversial.

We herein describe a case of HSE presenting with bilateral hippocampal lesions on MRI and simultaneous small cell lung carcinoma, and we discuss the possible relationships among HSE, PLE, and related forms of limbic encephalitis.

Case Report

A 75-year-old man experienced a sudden loss of consciousness on November 18, 1994. Ten days later, disorientation and partial seizures in the left hand were observed for several minutes. Thereafter, fever and abnormal behavior appeared. On November 29, the patient was admitted to our university hospital. On admission, the patient's temperature was 37.6°C, blood pressure was 140/60 mmHg, and pulse rate was 86/min. He showed a score of 10 points on the Japan Coma Scale; light reflex was prompt bilaterally; and meningeal irritation signs were absent. Deep tendon reflexes were normal, without Babinski reflexes, and recto-urinary disturbance was present.

His peripheral blood counts were normal: CRP 4.01 mg/dl, erythrocyte sedimentation rate 11 mm/h, and blood sugar 136 mg/dl. Serologic tests for syphilis were negative; serum fluorescent antibody (FA) I g G for herpes simplex virus (HSV) was 1 : 80; and enzyme immunoassay (EIA) IgG for HSV was 61.9. His cerebrospinal fluid (CSF) pressure was 170 mmH_2O; the fluid was clear and contained 10 cells/μl, 37 mg/dl protein, 70 mg/dl glucose, 24.7 pg/ml interleukin (IL)-6 (normal <9.7), and 6 pg/ml interferon (IFN)-γ (normal <46.6). CSF EIA IgG for HSV was 5.2, and serum HSV EIA IgG/CSF EIA IgG antibody ratio was 11.68 (positive <20). Polymerase chain reaction (PCR) for HSV was performed with DNA extracted from a 100 μl sample of CSF. The prim-

From the First Department (Neurology) of Internal Medicine and *the Internal Medicine, Kurume Medical Center, Kurume University School of Medicine, Kurume, **the Department of Pediatrics, Yamaguchi University School of Medicine, Ube and ***the Department of Neurology, Kanazawa Medical University, Kanazawa

Received for publication January 28, 2005; Accepted for publication May 11, 2005

Reprint requests should be addressed to Dr. Hiroshi Shoji, the First Department (Neurology) of Internal Medicine, Kurume University School of Medicine, 67 Asahimachi, Kurume 830-0011

ers were used at both the DNA polymerase and thymidine kinase gene regions of HSV type 1 (9). HSV type 1 DNA was detected in CSF at both gene regions. Anti-Hu and Ma2 antibodies were negative. Chest X-ray showed infiltration with swelling in the bilateral mediastinal lymph nodes. Brain CT was unremarkable, and axial T1- and T2-weighted MRI exhibited bilateral hippocampal lesions (Fig. 1).

Clinical course: Consciousness impairment progressed rapidly. The patient was diagnosed as having HSE, and acyclovir at 1.5 g per day was administered intravenously for 14 days. Phenytoin was also used to prevent convulsive seizures. Altered consciousness was prolonged, and convulsive seizures continued with fever and an increase of CRP. Vidarabine at 600 mg per day was added for 14 days. Three weeks after the initial MRI, a second MRI showed no change. At the same time, chest CT was carried out under the suspicion of lung carcinoma, and small cell carcinoma was confirmed by transbronchial biopsy. In mid-February 1995, a 25% dose of combined therapy for small cell carcinoma consisting of 150 mg carboplatin and 150 mg etoposide was started; the dose was kept low due to hepatic disturbance. Lymph node swelling in the mediastinum markedly decreased. In early March, the patient was transferred to another hospital, but his general status was worsening, and he died on April 24, 1995. Necropsy was not permitted.

Approximately ten years after the patient's death, because his case had raised the question of overlap between HSE and PLE, we tested for anti-Hu, Ma2, and Ma antibodies in the CSF from the patient that had been stored at –80°C. His CSF tested negative for the presence of these antibodies. At the same time, immunohistochemistry was performed on mouse brain sections using the stored CSF. The 6-μm-thick cryostat sections of mouse brain were sequentially reacted with CSF diluted to 1 : 100 in PBS and fluorescein isothiocianate (FITC)-labeled anti-human IgG. The immunohistochemistry study revealed that the neuronal cells in the cerebellum, in the Purkinje and molecular layers but not in the granular layer (Fig. 2), and the nucleus of most neurons of the cerebrum were highly labeled. Western blot analysis was conducted by using mouse cerebellum protein extracts (10 mg) (10). The blot was probed with the patient's CSF diluted to 1 : 10 in PBS, followed by incubation with anti-mouse IgG-alkaline phosphatase conjugate antibody. The patient's CSF IgG specifically recognized an approximately 29-kDa protein (Fig. 3).

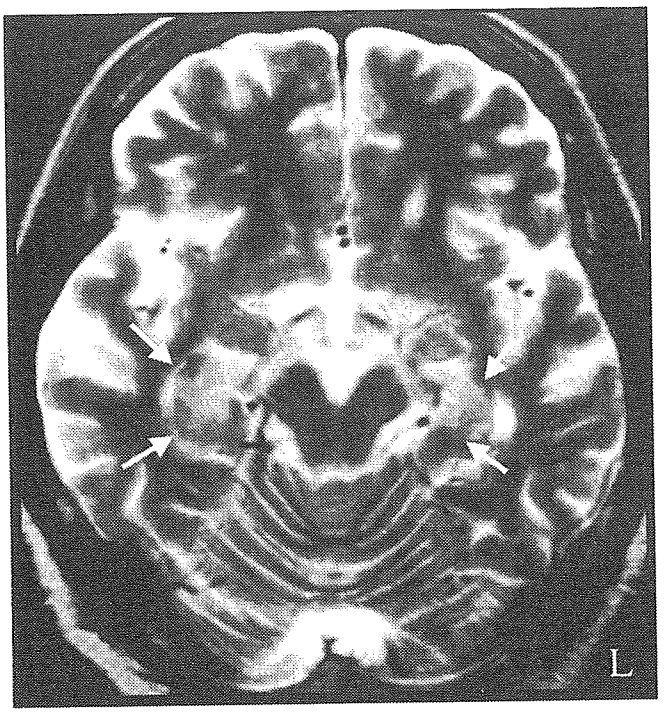

Figure 1. Approximate 20 days after onset, T2-weighted axial MRI (1.5 T superconducting magnet system, SE 4,000/88) revealed bilateral hippocampal lesions (arrows).

Figure 2. Section of mouse cerebellum immunolabeled with the patient's CSF. The neurons in the Purkinje and molecular layers of the cerebellum are highly labeled by the patient's CSF IgG (×100).

Discussion

The present HSE case, in which the HSV genome was proved in his CSF by PCR, was simultaneously complicated by small cell lung carcinoma, with MRI abnormalities localized to the bilateral hippocampi. In HSE, MRI lesions often progress unilaterally across the whole temporal lobe, and symmetrical limbic system lesions have been reported as being extremely rare (1–3). Non-herpetic ALE, a subgroup of limbic encephalitis that is characterized by MRI lesions in the bilateral hippocampi and amygdalae, negative on HSV PCR and EIA assay and without malignancy, has been reported (6–8). The levels of CSF IL-6 and IFN-γ in cases of non-herpetic ALE were found to be significantly lower than those in cases of HSE (11, 12).

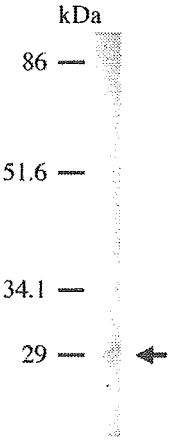

Figure 3. Immunoblot of mouse brain protein extracts probed with the patient's CSF, which recognized an approximately 29-kDa protein (arrow).

Sharshar et al (13) have reported a similar autopsy case of HSE in which the HSV genome was detected in the neuronal nuclei or cytoplasm by PCR. In their case, pathologically different characteristic findings of both HSE and PLE were observed with the anti-Hu antibody. They proposed the possibility of a link between the two diseases; that is, HSV infection may induce the production of anti-neural antibodies, or a specific protein in the limbic system may be involved in the pathogenesis of both HSE and PLE (14). Our HSE case presented with bilateral hippocampal lesions on MRI, and the CSF cytokine findings of elevated IL-6 and normal IFN-γ were compatible with those in non-herpetic ALE (11). Simultaneously, our case was complicated by small cell lung carcinoma, and a new anti-neuronal cell antibody in the CSF was identified. The antibody differs from well-known anti-neuronal cell antibodies associated with PLE, such as anti-Hu, anti-Ta (Ma2), anti-Ma, anti-amphiphysin, and anti-CRMP-5 antibodies. Our findings suggest that HSE, non-herpetic ALE, and PLE can overlap.

Recently, various causes have been clarified for the pathogenesis of ALE. In terms of mild CSF pleocytosis and MRI lesions in the bilateral hippocampi, our case of ALE due to HSV may resemble those caused by human herpesvirus 6 after stem cell transplantation (15, 16). Moreover, reversible ALE with glutamate receptor (Glu R) ε2, and ALE associated with ovarian teratoma containing immature nervous system tissues, as well as those with potassium channel antibodies, have been reported (17–20). Additional cases are needed to elucidate the relationships among HSE, PLE, and related forms of limbic encephalitis, including non-herpetic ALE.

Acknowledgments: This study was supported by a grant from the Cognitive and Molecular Research Institute of Brain Diseases, Kurume University, Japan. This paper was presented at the 8th Japanese Neuroinfectious Diseases Congress, Yamaguchi, October 2003.

References

1) Schroth G, Gawehn J, Thron A, Vallbracht A, Voigt K. Early diganosis of herpes simplex encephalitis by MRI. Neurology **37**: 179–183, 1987.
2) Demaerel P, Wilms G, Robberecht W, et al. MRI of herpes simplex encephalitis. Neuroradiology **34**: 490–493, 1992.
3) Kapur N, Barker S, Burrows EH, et al. Herpes simplex encephalitis: long term magnetic resonance imaging and neuropsychological profile. J Neurol Neurosurg Psychiatry **57**: 1334–1342, 1994.
4) Voltz R, Gultekin SH, Rosenfeld MR, et al. A serologic marker of paraneoplastic limbic and brain-stem encephalitis in patients with testicular cancer. N Engl J Med **340**: 1788–1795, 1999.
5) Gultekin SH, Rosenfeld MR, Voltz R, Eichen J, Posner JB, Dalmau J. Paraneoplastic limbic encephalitis: neurological symptoms, immunological findings and tumour association in 50 patients. Brain **123**: 1481–1494, 2000.
6) Kusuhara T, Shoji H, Kaji M, Ayabe M, Hino H. Non-herpetic acute limbic encephalitis. Rinshou Shinkeigaku **34**: 1083–1088, 1994 (in Japanese, Abstract in English).
7) Shoji H, Koga M, Kusuhara T, et al. Differentiation of herpes simplex virus 1 and 2 in cerebrospinal fluid of patients with HSV encephalitis and meningitis by stringent hybridization of PCR-amplified DNAs. J Neurol **241**: 526–530, 1994.
8) Kaji M, Kusuhara T, Ayabe M, Hino H, Shoji H, Nagao T. Survey of herpes simplex virus infections of the central nervous system, including acute disseminated encephalomyelitis, in the Kyushu and Okinawa regions of Japan. Mult Scler **2**: 83–87, 1996.
9) Klapper PE, Cleator GM, Dennett C, Lewis AG. Diagnosis of herpes encephalitis via Southern blotting of cerebrospinal fluid DNA amplified by polymerase chain reaction. J Med Virol **32**: 261–264, 1990.
10) Towbin H, Staehelin T, Gordon J. Electrophoretic transfer of proteins from polyacrylamide gels to nitrocellulose sheets: procedure and some applications. Proc Natl Acad Sci USA **76**: 4350–4354, 1979.
11) Asaoka K, Shoji H, Nishizaka S, et al. Non-herpetic acute limbic encephalitis. CSF cytokines and MRI findings. Intern Med **43**: 42–48, 2004.
12) Shoji H, Asaoka K, Ayabe M, Ichiyama T, Sakai K. Non-herpetic acute limbic encephalitis. A new subgroup of limbic encephalitis? Intern Med **43**: 348, 2004.
13) Sharshar T, Auriant I, Dorandeu A, et al. Association of herpes simplex virus encephalitis and paraneoplastic encephalitis—a clinico-pathological study. Ann Pathol **20**: 249–252, 2000.
14) Nagashima K, Kobayashi Y, Kojima H, Hasegawa H, Kurata T. Herpes encephalitis and paraneoplastic limbic encephalitis. Neuropathology **18**: 215–221, 1998.
15) Wainwright MS, Martin PL, Morse RP, et al. Human herpesvirus 6 limbic encephalitis after stem cell transplantation. Ann Neurol **50**: 612–619, 2001.
16) Yoritaka A, Ohta K, Akiyama H, Kishida S. Limbic encephalitis probably due to human herpesvirus 6 after stem cell transplantation: a report of 3 cases. Neuroinfection **10**: 88–93, 2005.
17) Nemoto H, Takahashi Y, Yuasa T. Autoantibody-mediated acute reversible limbic encephalitis (AMED-ARLE). Neuroinfection **10**: 44–46, 2005 (in Japanese).
18) Watanabe Y, Shimizu Y, Ooi S, Tanaka K, Inuzuka T, Nakashima K. Steroid-responsive limbic encephalitis. Intern Med **42**: 428–432, 2003.
19) Vincent A, Buckley C, Schott JM, et al. Potassium channel antibody-associated encephalopathy: a potentially immunotherapy-responsive form of limbic encephalitis. Brain **127**: 701–712, 2004.
20) Munakata S, Nagumo K, Masaoka N, Sugitani M, Kojima S. Non-herpetic acute limbic encephalitis recovered before the growing of the ovarian teratoma. Shinkeinaika **59**: 112–116, 2003 (in Japanese).

Original Paper

Pathobiology

Pathobiology 2005;72:108–116
DOI: 10.1159/000084113

Received: May 26, 2004
Accepted: July 30, 2004

Myosin Loss in Denervated Rat Soleus Muscle after Dexamethasone Treatment

Hideo Horinouchi Toshihide Kumamoto Noriyuki Kimura
Hidetsugu Ueyama Tomiyasu Tsuda

Division of Neurology and Neuromuscular Disorders, Department of Brain and Nerve Science,
Oita University Faculty of Medicine, Oita, Japan

Key Words
Atrogin-1 · Critical illness myopathy · Myosin heavy chain · Proteasome · Ubiquitin-proteasome pathway

Abstract
Objective: Critical illness myopathy (CIM) is an acute myopathy that appears in the setting of critical illness or during exposure to corticosteroids and neuromuscular blocking agents. Its pathological feature is selective loss of thick myosin filaments. Our aim is to gain further insight into the pathomechanism of myosin loss in this myopathy. ***Methods:*** To clarify the expression of myosin heavy chain (MHC) and ubiquitin ligase atrogin-1 in this myopathy, histological, immunohistochemical, SDS-PAGE, and semiquantitative reverse transcriptase-polymerase chain reaction studies were performed on innervated and denervated rat soleus muscles after saline and dexamethasone treatments. ***Results:*** Denervated muscles from dexamethasone-treated rats showed marked MHC loss. The mRNA expression of ubiquitin ligase atrogin-1 was significantly increased in denervated dexamethasone-treated muscles, suggesting that the ubiquitin-proteasome pathway plays an important role in muscular wasting in CIM. Furthermore, mRNA levels of MHC I, a myosin isoform, were decreased in the denervated dexamethasone-treated muscles. ***Conclusion:*** Our findings suggest that an altered transcription rate of myosin, as well as the upregulation of multiple ubiquitin ligases, may be responsible for selective myosin loss in this myopathy.

Introduction

Critical illness myopathy (CIM) is an acute myopathy that appears during critical illness [1]. Most often severe weakness occurs during the initial recovery from an acute illness. Since Macfarlane and Rosenthal [2] reported the first case of acute quadriplegic myopathy in 1977, many other CIM cases have been reported throughout the world. Although of unknown etiology, three main risk factors appear to be associated with CIM: exposure to corticosteroids, exposure to neuromuscular blocking agents, and a severe systemic illness such as sepsis, renal failure, or respiratory failure. The pathological hallmark of CIM is loss of thick myosin filaments in the skeletal muscle fibers of patients with this myopathy [1, 3–10], but the pathomechanism of this myosin loss is still not known.

Previous reports showed that selective myosin loss occurred in denervated soleus and plantar muscles of rats receiving simultaneous high doses of corticosteroids [11–13]. The pathological changes in those rats are similar to

KARGER
Fax +41 61 306 12 34
E-Mail karger@karger.ch
www.karger.com

1015–2008/05/0723–0108$22.00/0

Accessible online at:
www.karger.com/pat

Dr. Hideo Horinouchi
Division of Neurology and Neuromuscular Disorders
Department of Brain and Nerve Science, Oita University Faculty of Medicine
Idaigaoka 1-1, Hasama, Oita 879-5593 (Japan)
Tel. +81 975 86 5814, Fax +81 975 49 6502, E-Mail horinouc@oita-med.ac.jp

those in human CIM induced by treatment with high-dose corticosteroids and neuromuscular blocking agents and which has the same properties as pharmacological muscle denervation [1, 4]. A mechanism similar to that in experimental rats is speculated to be responsible for selective myosin loss in skeletal muscle from CIM patients. Steroid-treated, denervated rats, therefore, provide a good model for analysis of the mechanism of muscle fiber degradation in CIM, especially myosin loss.

Like other tissues, muscle has at least three different pathways for protein breakdown: proteolysis by lysosomal proteases such as cathepsins, proteolysis by nonlysosomal, intracellular Ca^{2+}-dependent proteases such as calpain, and proteolysis by nonlysosomal, ATP-ubiquitin-dependent proteolytic protease, functioning as a multicatalytic protease complex (proteasome) [14, 15]. Previous studies suggested that the ubiquitin-proteasome proteolytic pathway may have a central role in muscle fiber degradation in CIM [6, 10]. Proteins degraded in this proteolytic pathway first are conjugated to multiple molecules of ubiquitin and then degraded into small peptides by the multicatalytic 26S proteasome [14, 16]. The catalytic core of 26S proteasome is the 20S proteasome, a barrel-shaped particle composed of four stacked rings with seven subunits in each ring [17]. The two outer rings are comprised of α-subunits (RC2, RC3, RC8, etc.). The α-subunits function in the interaction between the 20S proteasome and various regulators.

The ubiquitination of muscle protein is regulated by multiple enzymes, including ubiquitin ligases (E3), e.g., E3α [18]. Recent findings suggest that in addition to E3α other ubiquitin ligases, in particular atrogin-1/muscle atrophy F-box (MAFbx) [19], and muscle RING finger 1 (MURF 1) [20] play a key role in the generation of muscle atrophy. Gene expressions of atrogin-1/MAFbx and MURF 1 were found to be increased in rat skeletal muscles during sepsis, suggesting that atrogin-1/MAFbx may participate in the development of muscle wasting during sepsis via the ubiquitin-proteasome pathway [21]. We, therefore, hypothesize that CIM upregulates the gene expression of the newly described ubiquitin ligase, atrogin-1/MAFbx.

A previous study suggested that CIM decreases the gene transcription of myosin [9] with or without degradation. Myosin consists of two subunits, the myosin heavy chain (MHC) and myosin light chains. At least four different MHC isoforms: MHC I, MHC IIa, MHC IIx, and MHC IIb, are expressed at high levels in rat limb muscles. In the rat soleus muscles, only two MHC isoforms, MHC I and MHC IIa are expressed. The levels of MHC I isoform expression are markedly higher than that of MHC IIa [22]. Despite high expression of the MHC I isoform in rat soleus muscle (electrophoretically separated 89 ± 3%), MHC I gene expression in denervated muscles after dexamethasone treatment has not been studied.

To clarify the expression of myosin and atrogin-1/MAFbx in CIM muscles, histological, immunohistochemical, biochemical, and semi-quantitative reverse transcriptase-polymerase chain reaction (RT-PCR) studies were performed on innervated and denervated rat soleus muscles after saline and dexamethasone treatments.

Materials and Methods

Animals and Muscles

Twenty adult male Sprague-Dawley rats (initial body weight 300–350 g) were anesthetized with diethyl ether. The right hind leg was denervated by ligation of the sciatic nerve midway between the popliteal fossa and sciatic notch. Dexamethasone (5 mg/kg of body weight) or an identical volume of saline was injected intraperitoneally daily beginning on the day of denervation. After the initial injection, each rat was weighed daily. The animals were sacrificed by decapitation on days 2 and 7. Both the right (denervated) and left (innervated) soleus muscles were removed from the saline- and dexamethasone-treated rats. Each muscle was weighed. Four groups of muscles were established and each group consisted of 5 rats; control, denervated, dexamethasone-treated, and denervated plus dexamethasone-treated muscles. These muscles were frozen rapidly in isopentane chilled with liquid nitrogen, then stored at -80° C until used.

Histological, Histochemical, and Immunohistochemical Studies

Transverse cryostat sections, 10 μm thick, were stained with hematoxylin-eosin and adenosine triphosphatase after incubation in acid (pH 4.3 and 4.6) and alkaline (pH 10.3) buffers, as described elsewhere [23].

For immunohistochemistry, unstained frozen sections were fixed in acetone for 10 min and then incubated for 15 min in phosphate-buffered saline (PBS) containing 10% (wt/vol) fat-free dried milk. After washing, the specimens were incubated with primary antibody for 1 h at room temperature. Monoclonal antimouse antibodies for slow myosin (Chemicon, Temecula, Calif., USA) and fast myosin (Sigma, St. Louis, Mo., USA) were diluted 1:800 in PBS, containing 1% fat-free dried milk and 0.1% Tween 20 (TPBS). After washing three times in TPBS, the specimens were incubated with 1:1000 dilution of biotinylated anti-mouse IgG for 30 min. Sites of antibody binding were visualized by staining with 3,3′-diaminobenzidine tetrahydrochloride with a Vectastain ABC Kit (Vector Labs., Burlingame, Calif., USA), and the sections were lightly counterstained with hematoxylin. Immunostaining was specific because no staining was obtained when sections were allowed to react without first-layer antibodies or with normal mouse serum substituted for first-layer antibodies.

Sodium Dodecyl Sulfate Polyacrylamide Gel Electrophoresis (SDS-PAGE)

For this electrophoresis, ten to twenty 10-μm-thick transverse cryostat sections sliced from the rat soleus muscle were thawed and homogenized in 400–800 μl of SDS sample buffer composed of 0.125 *M* Tris-HCl buffer (pH 6.8), 10% 2-mercaptoethanol, 4% (wt/vol) SDS, 10% sucrose, and 0.004% bromophenol blue. SDS-PAGE was done with 10% acrylamide separating gels according to the method of Laemmli [24]. The gels were stained with Coomassie blue. Scanning densitometry with an Epson GT8000 scanner (Epson, Tokyo, Japan) was used to determine the peak areas of the actin and MHC bands. Data, given in relative units, were analyzed with the software NIH image (version 1.62) in a Macintosh computer (Apple Computer Cupertino, Calif., USA). Protein was measured by the method of Lowry et al. [25].

Semiquantitative RT-PCR

Total RNAs were isolated from 40 cryostat sections, 20 μm thick, of each experimental rat soleus muscle by acid guanidinium thiocyanate/phenol buffer (Isogen; Nippon Gene, Tokyo, Japan), used according to the manufacturer's instructions [26]. One microgram of total RNA [for MHC I, glycerol aldehyde 3-phosphate dehydrogenase (GAPDH) was the standard] and 0.3 μg of total RNA (for atrogin-1, RC3 and GAPDH as the standard) from each soleus muscle was reverse transcribed into first-strand complementary DNA (cDNA) in a 20-μl volume of 5 × first strand buffer (250 m*M* Tris-HCl, pH 8.3, 375 m*M* KCl, 15 m*M* $MgCl_2$), 10 m*M* dithiothreitol, 1 m*M* dNTPs, 1 μg of oligo-$(dT)_{12-18}$ primer (Pharmacia Biotech, Tokyo, Japan), 40 units of RNasin (Promega, Madison, Wisc., USA), and 200 units of Moloney murine leukemia virus reverse transcriptase (Gibco BRL, Gaithersburg, Md., USA). PCR primer construction was based on published nucleotide sequences of the mouse atrogin-1 gene (sense primer: Nos. 502–521, 5′-GTCGCAGCCAAGAAGAGAAA-3′; antisense primer: Nos. 644–663, 5′-GGCAGTCGAGAAGTCCAGTC-3′) [19], the rat RC3 gene (sense primer: Nos. 201–218, 5′-GGAGCCCATAACCAAGCA-3′ antisense primer: Nos. 375–392, 5′-GGACGAACACCACCTGAC-3′) [27], the rat MHC I gene (sense primer: 5′-GAAGGCCAAGAAGGCCATC-3′; antisense primer: 5′-GGTCTCAGGGCTTCACAGGC-3′) [28], and the rat GAPDH gene (sense primer: 5′-TGCCAAAAGGGTCATCATCT-3′; antisense primer: 5′-GCCAGCCCCAGCATCAAAGG-3′) [29]. RT-PCR reactions took place in a final 50-μl volume in a DNA thermal cycler (PTC-200, MJ Research, Osaka, Japan) [30]. Each PCR reaction mixture contained 1 μl of cDNA, 10 × PCR buffer (100 m*M* Tris-HCl, pH 8.3, 500 m*M* KCl, 15 m*M* $MgCl_2$), 200 m*M* dNTP, 0.2 μ*M* of each primer set, and 1 unit of Taq DNA polymerase (Qiagen, Valencia, Calif., USA). The following conditions were used for amplification: denaturation at 94°C for 1 min, annealing at 50°C for 2 min, and extension at 72°C for 1 min for atrogin-1, RC3 and GAPDH; and denaturation at 95°C for 45 s, annealing at 52°C for 50 s, and extension at 72°C for 50 s for MHC I. The number of cycles was adjusted to allow product detection in the exponential range of amplification. Cycle numbers were 26 for atrogin-1 and RC3, 32 for MHC I, and 24 for GAPDH. Because the target sequences of these primers were located on different exons, only a proper RT reaction resulted in the amplification of a PCR product of the correct fragment size. Respective sizes of the amplified products were 162, 192, 596, and 556 base pairs for atrogin-1, RC3, MHC I and GAPDH. After 1.5 or 3.0% agarose gel electrophoresis, scanning densitometry (Epson GT-8000 scanner) was used to determine the peak areas and the relative amount of mRNA in the ethidium bromide-stained bands. The intensity of each band was quantified by NIH image (version 1.61) in a Macintosh computer. Atrogin-1, RC3, and MHC I mRNA levels were normalized in relation to the GAPDH mRNA level.

Statistical Analysis

All data are presented as means ± standard error. Statistical differences were calculated by use of the unpaired Student t test.

Significance was accepted at the level of $p < 0.05$.

Results

Body Weights and Muscle Weights

Body weights of the dexamethasone-treated rats decreased during the experiment. The respective mean body weights of the saline- and dexamethasone-treated rats were 366 ± 11.48 and 260 ± 14.1 g during day 7 after the initial injection, respectively. The body weights of the dexamethasone-treated rats were significantly lower than those of the controls on day 7. The mean muscle weights of the denervated soleus muscles from saline- and dexamethasone-treated rats were significantly lower than those of the innervated muscles of both rats on day 7 after the initial injection (innervated, saline-treated muscle: 0.152 ± 0.004 g; innervated, dexamethasone-treated muscle: 0.147 ± 0.004 g; denervated, saline-treated muscle: 0.091 ± 0.004 g; denervated, dexamethasone-treated muscles: 0.069 ± 0.006 g).

Histological, Histochemical, and Immunohistochemical Findings

Pathological findings on each test day for the innervated and denervated soleus muscles from the saline- and dexamethasone-treated rats were similar to those described previously [11, 13]. Briefly, most left innervated soleus muscles from both experimental rat groups appeared normal and predominantly had type 1 fibers. In contrast, the denervated muscles of both groups showed marked neurogenic changes of various degrees of severity on day 7 after denervation (fig. 1a, b). In the denervated, dexamethasone-treated muscles, the myosin ATPase-staining activity in some muscle fibers was often decreased (data not shown). On immunohistochemistry, all fibers of the innervated muscles from both groups and the denervated muscles from saline-treated rats on day 7 were normally labeled by antifast and antislow MHC antibodies (fig. 1c, e). In the denervated muscles from dexamethasone-treated rats, immunohistochemical labeling

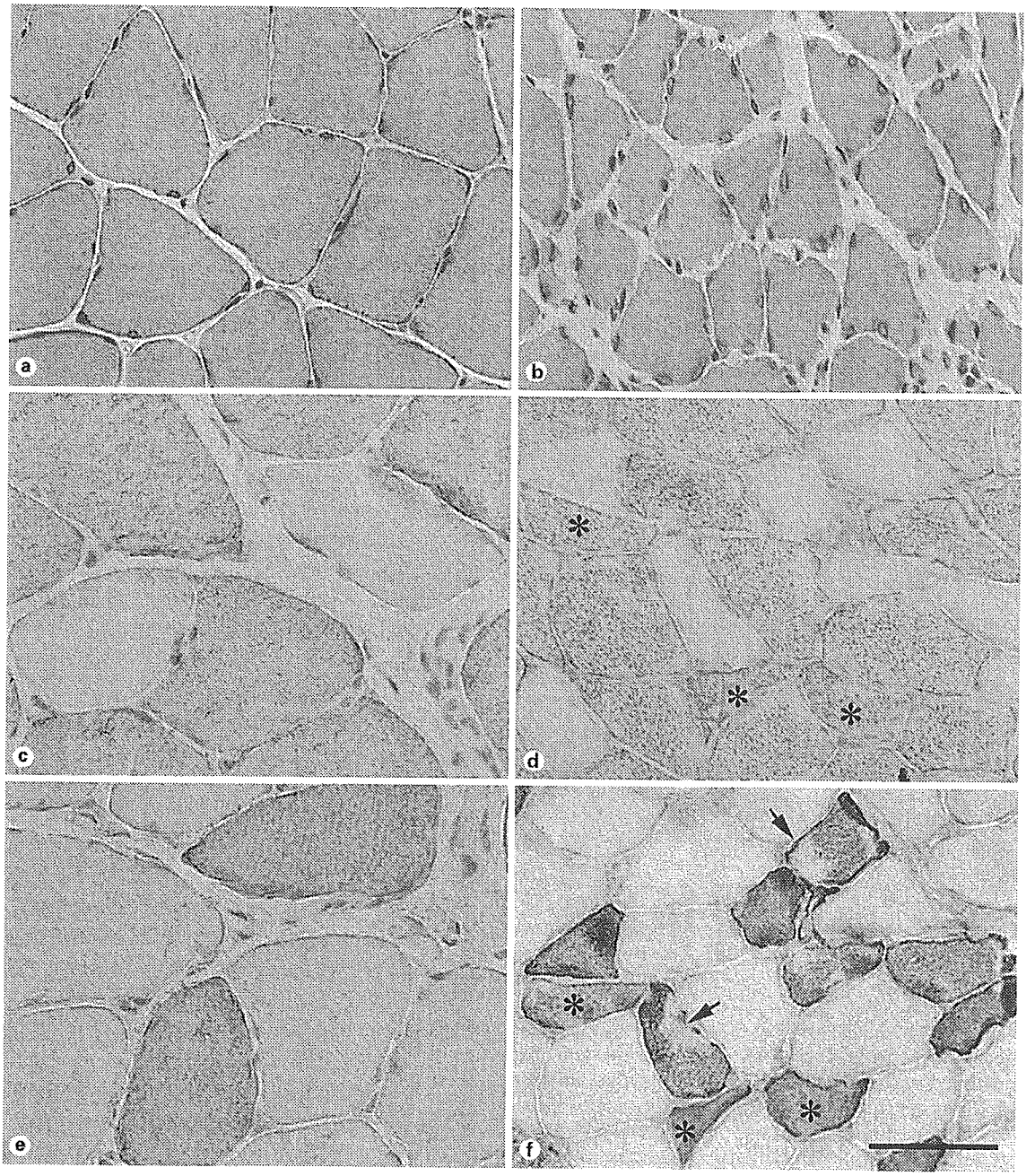

Fig. 1. Cross-sections of rat soleus muscles after 7 days of saline or dexamethasone treatment. The innervated muscle of a saline-treated rat has a normal appearance (**a**). In contrast, the denervated dexamethasone-treated muscle shows moderate muscle fiber atrophy (**b**). Immunohistochemical labeling for fast and slow MHC is well-preserved in the innervated muscle of a saline-treated rat (**c**, **e**). The denervated, dexamethasone-treated muscle shows less intense stain of slow MHC (**d**) and irregular reduction in the intensity of staining of fast MHC (**f**, arrow) in several fibers on day 7. Some fibers that contain both fast and slow MHC are type 2C fibers (asterisk). **a**, **c**, **e** Innervated muscle from a saline-treated rat. **b**, **d**, **f** Denervated muscle from a dexamethasone-treated rat. Hematoxylin and eosin (**a**, **b**), immunostainings with anti-slow (**c**, **d**) and anti-fast (**e**, **f**) MHC monoclonal antibodies. Bar = 50 μm.

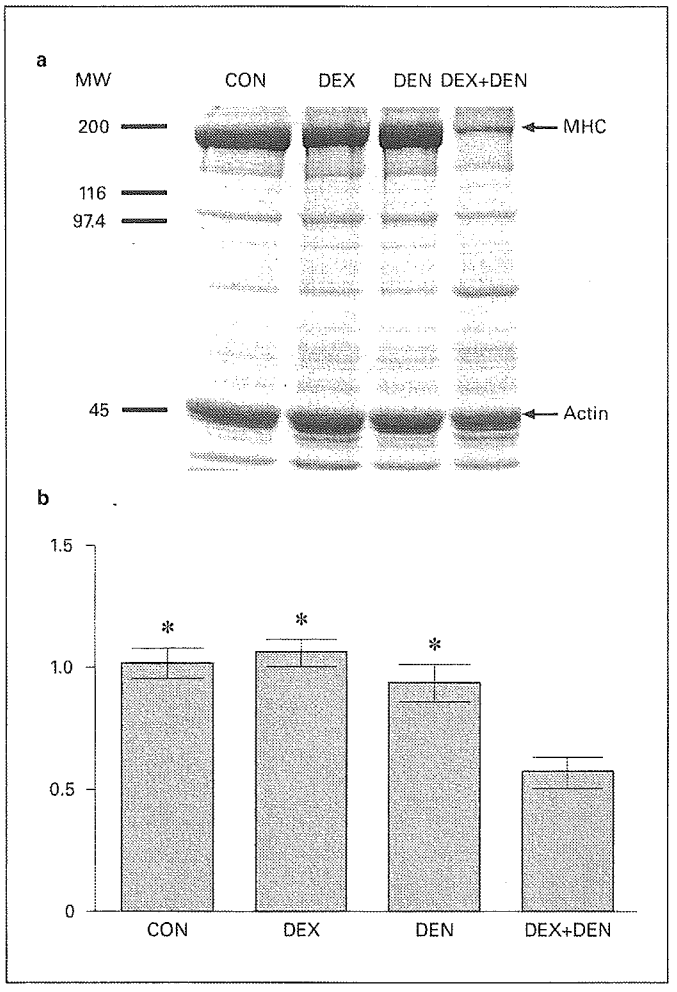

Fig. 2. a SDS-polyacrylamide slab gel patterns in innervated and denervated rat soleus muscles after 7 days of saline or dexamethasone treatment. The intensity of the band corresponding to the myosin heavy chain (MHC) is decreased markedly in the denervated dexamethasone-treated muscles. **b** Densitometric quantification of the MHC and actin bands in innervated and denervated rat soleus muscles on day 7 of saline or dexamethasone treatment. The MHC/actin ratio shows a significant decrease in the denervated, dexamethasone-treated muscle as compared with the innervated, saline-treated (control) muscle, the dexamethasone-treated muscle, and the denervated, saline-treated muscle (vs. control muscles, $p < 0.0001$; vs. the innervated, dexamethasone-treated muscles, $p < 0.0001$; vs. the denervated, saline-treated muscles, $p < 0.0001$). MW = Molecular weight; CON = controls; DEX = innervated muscles of dexamethasone-treated rats; DEN = denervated muscles of saline-treated rats; DEX + DEN = denervated muscles of dexamethasone-treated rats. * $p < 0.0001$; vs. the denervated, dexamethasone-treated muscle.

for fast and slow MHC was less intense and showed focal reduced reactivity in several fibers (fig. 1d, f).

SDS-PAGE

Electrophoretic protein patterns of the innervated, dexamethasone-treated muscles and denervated, saline-treated muscles were similar to those of the innervated muscles of the saline-treated rats (control). The intensity of the band corresponding to MHC was markedly low in the denervated muscles of the dexamethasone-treated rats (fig. 2a). Because there was no consistent depletion of actin, the MHC/actin ratio was used as a relative measure of MHC depletion. The mean of the MHC/actin ratios for all the experimental rats on day 7 was 1.008 ± 0.029 (innervated; control), 1.052 ± 0.003 (denervated) for the saline-treated muscles. It was 0.925 ± 0.007 (innervated) and 0.560 ± 0.065 (denervated) for the dexamethasone-treated muscles, significantly lower in the denervated, dexamethasone-treated muscles (fig. 2b). There were no statistical differences between the other experimental muscles and the control muscles.

Semiquantitative RT-PCR

PCR amplification without reverse transcription with extract RNA as the template was used to test for possible contamination of chromosomal DNA during DNA extraction. No bands appeared during 24–32 PCR cycles, evidence of the absence of contaminating DNA.

Atrogin-1, RC3, and MHC I mRNA were expressed constitutively in the innervated and denervated muscles from the saline- and dexamethasone-treated rats. The mRNA levels of the genes are given in figures 3 and 4. Scanning densitometry showed a significant increase in the expression of atrogin-1 in the denervated muscles of the saline- and dexamethasone-treated rats as compared with the contralateral, innervated muscles of both groups on days 2 and 7 (fig. 3a). Atrogin-1 mRNA levels in denervated muscles of dexamethasone-treated rats were significantly higher than those in saline-treated rats on days 2 and 7 (fig. 3b). RC3 gene expression tended to be upregulated in both types of denervated soleus muscles on day 2 relative to the control muscles, but the difference was not significant (fig. 3b).

Figure 4 shows the expression levels of MHC I mRNA in innervated and denervated muscles from the saline- and dexamethasone-treated rats. On day 7, the MHC I mRNA level has decreased significantly in the denervated muscles of the saline- and dexamethasone-treated rats as compared with the contralateral, innervated muscles of both groups, decreasing to 45 and 13%, respectively, of

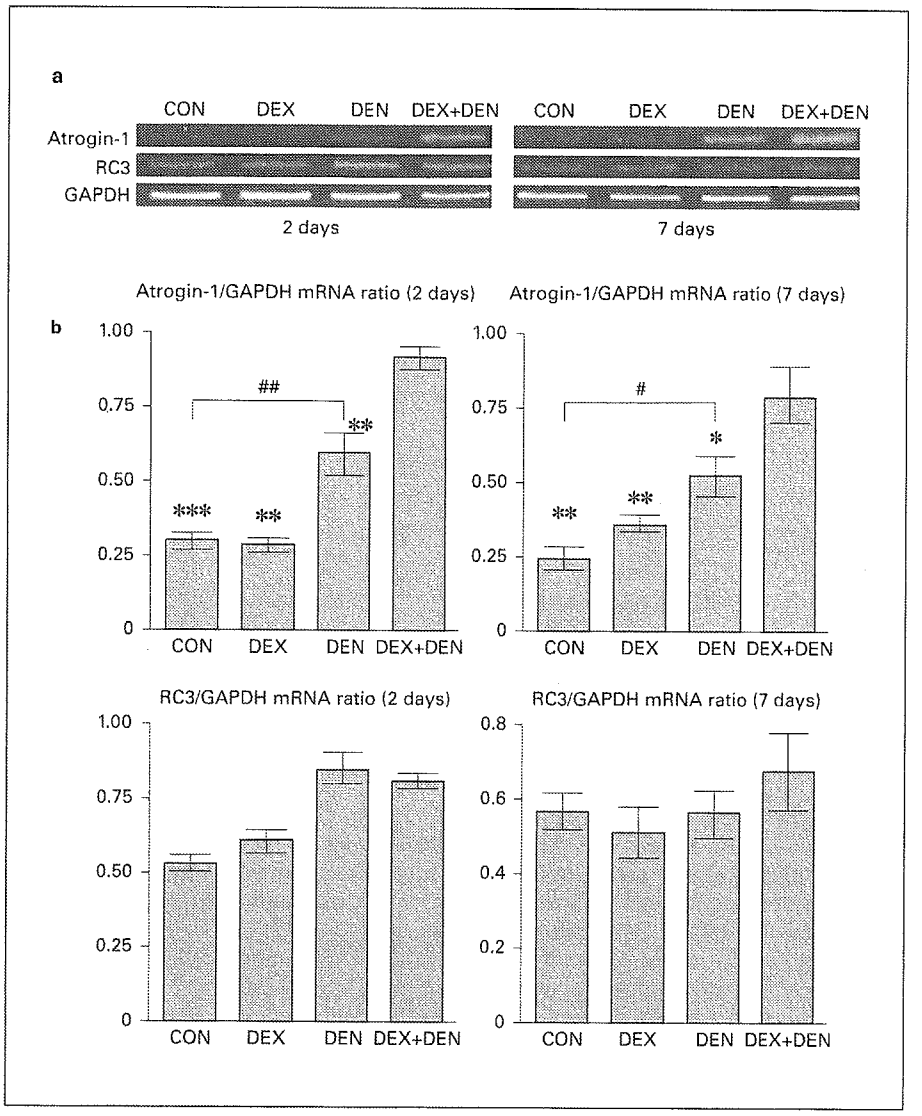

Fig. 3. a Semiquantitative analysis based on RT-PCR of the relative expression of atrogin-1, RC3, and GAPDH mRNA in innervated and denervated muscles on days 2 and 7 of saline or dexamethasone treatment. Ten microgram of the PCR products was subjected to 3.0% agarose gel electrophoresis, the gels stained with ethidium bromide, and the stain made visible by illumination with ultraviolet light. **b** Densitometric quantification of atrogin-1 and RC3 mRNA expression in each experimental muscle type on days 2 and 7. Scanning densitometry shows increased expression of atrogin-1 mRNA in the denervated muscles of both groups as compared with the innervated saline-treated (control) muscles (denervated, saline-treated muscles vs. control, $p < 0.01$ on day 2, $p < 0.05$ on day 7; denervated, dexamethasone-treated muscles vs. control, $p < 0.0001$ on day 2, $p < 0.01$ on day 7). mRNA expression is significantly higher in the denervated muscles after dexamethasone treatment than after saline treatment and in the innervated, dexamethasone-treated muscles (vs. denervated, saline-treated muscles, $p < 0.01$ on day 2, $p < 0.05$ on day 7; vs. innervated, dexamethasone-treated muscles, $p < 0.0001$ on day 2, $p < 0.01$ on day 7). MW = Molecular weight; CON = controls; DEX = innervated muscles of dexamethasone-treated rats; DEN = denervated muscles of saline-treated rats; DEX + DEN = denervated muscles of dexamethasone-treated rats. * $p < 0.05$, ** $p < 0.01$, *** $p < 0.0001$ vs. the denervated, dexamethasone-treated muscles. # $p < 0.05$, ## $p < 0.01$; control vs. the denervated, saline-treated muscles.

the control muscle values. Levels were significantly lower in the denervated muscles of dexamethasone-treated rats than in their innervated muscles.

Discussion

In the present study, we found severe volume loss in dexamethasone- and to a lesser extent in saline-treated rat soleus muscles after denervation as compared with contralateral, innervated muscles of both rats. In denervated, dexamethasone-treated muscles, histological, immunohistochemical, and biochemical findings showed severe muscle atrophy and decreased MHC. These pathological and biochemical findings are very similar to those for human CIM [1, 11, 12] induced by treatment with high-dose corticosteroids and neuromuscular blocking agents [1, 4]. These experimental rats are confirmed to be a good CIM model. There are reports on the mechanism of myosin loss in denervated muscles of dexamethasone-treated rats. Rouleau et al. [13] suggested that decreased myosin synthesis probably is a significant contributor to the preferential myosin depletion in this myopathy because of reduced muscle protein synthesis, primarily owing to decreased numbers of ribosomes produced by excessive glucocorticoid and denervation treatments [13], but they did not explain the preferential loss of myosin nor did they study myosin degradation.

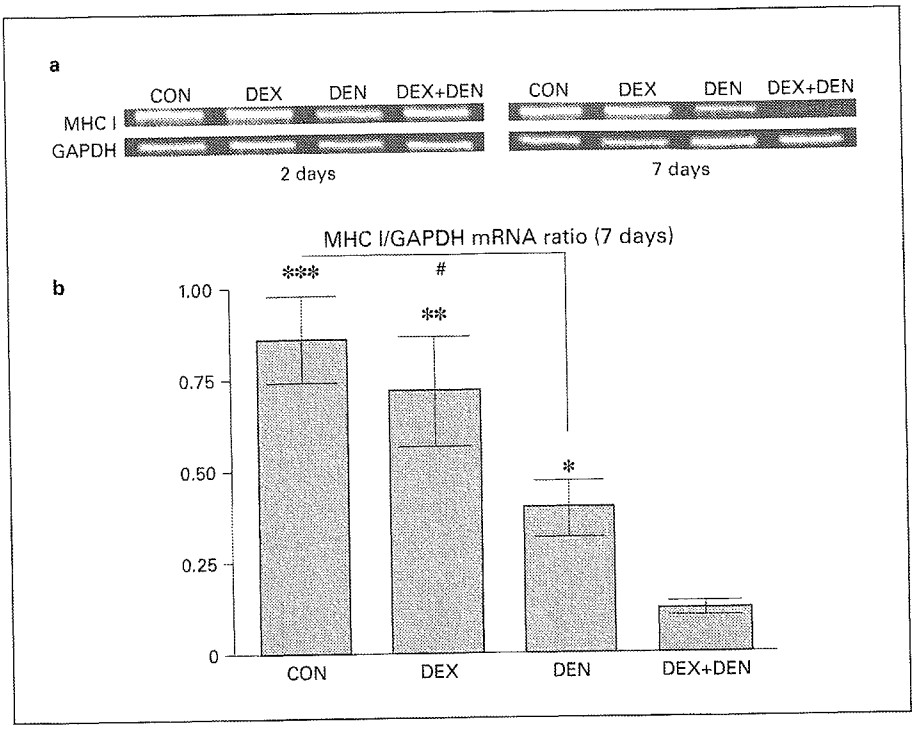

Fig. 4. a Semiquantitative RT-PCR analysis of the relative expression of myosin heavy chain (MHC) I and GAPDH mRNA in innervated and denervated muscles on days 2 and 7 of saline or dexamethasone treatment. Ten microgram of PCR products was subjected to 1.5% agarose gel electrophoresis. The gels were stained with ethidium bromide, and the stain made visible by illumination with ultraviolet light. **b** Densitometric quantification of MHC I mRNA expression in each muscle specimen on day 7. Scanning densitometry shows decreased expression of this mRNA in the denervated muscles of both groups as compared with the innervated saline-treated (control) muscles (vs. the denervated, saline-treated muscles, $p < 0.05$; vs. the denervated, dexamethasone-treated muscles, $p < 0.001$). mRNA expression is significantly lower in the denervated muscles after dexamethasone treatment than in the saline-treated and the innervated, dexamethasone-treated muscles (vs. the denervated, saline-treated muscles, $p < 0.01$ on day 2, $p < 0.05$ on day 7; vs. the innervated, dexamethasone-treated muscles, $p < 0.01$). MW = Molecular weight; CON = controls; DEX = innervated muscles of dexamethasone-treated rats; DEN = denervated muscles of saline-treated rats; DEX + DEN = denervated muscles of dexamethasone-treated rats. * $p<0.05$, ** $p<0.01$, *** $p<0.001$ vs. the denervated, dexamethasone-treated muscles. # $p<0.05$; control vs. the denervated, saline-treated muscles.

We found decreased MHC I mRNA levels in denervated soleus muscles from saline- and dexamethasone-treated rats. On day 7, the MHC I mRNA levels of the denervated muscles from both saline- and dexamethasone-treated rats respectively were 45 and 13% those of the innervated muscles from the saline-treated rats (control muscle). This suggests that steroid treatment may promote the downregulation of the MHC I gene owing to denervation. Previously, only denervation treatment was reported to lead to significant decreases in MHC proteins and MHC mRNA in rat muscles [31]. Our findings suggest that the myosin loss may be due to changes in myosin itself at the molecular level (e.g., a decreased transcription rate and decreased mRNA stability), but increased myofibrillar proteolysis also may be involved [32, 33].

Myosin is degraded by the lysosomal proteases cathepsin B and L and by nonlysosomal proteases such as calpain and proteasomes. Recent evidence indicates that the ubiquitin-proteasome proteolytic pathway may function in the breakdown of skeletal muscle myofibrillar proteins, including actin and myosin, and in such physiological and pathological conditions as denervation, starvation, metabolic acidosis, cancer, and sepsis [34–39]. Previous findings suggest that in addition to E3α, another ubiquitin ligase, atrogin-1/MAFbx, may regulate the muscle protein breakdown under various catabolic conditions and be more important than E3α in the development of muscle wasting in proteolysis via the ubiquitin-proteasome pathway [19, 20]. The atrogin-1/MAFbx-expressing gene is only present in muscle tissues, indicative that this

ubiquitin ligase is muscle specific. Atrogin-1/MAFbx specifically regulates protein breakdown in skeletal muscles under the catabolic conditions of immobilization, denervation, hind limb suspension, treatment with interleukin-1 or dexamethasone, sepsis, fasting, and renal failure [19–21]. We found that gene expression of the newly described ubiquitin ligase, atrogin-1, increased significantly in the denervated soleus muscles of saline- and dexamethasone-treated rats. The mRNA levels of the gene in the denervated muscles from the saline- and dexamethasone-treated rats on day 7 respectively were two and three times those in the control muscles. This speculates that ubiquitin ligase atrogin-1 protein expression is increased by denervation treatment alone and has a specific role in myofibrillar protein degradation in denervated muscles of saline- and dexamethasone-treated rats [19–21]. Furthermore, the mRNA for atrogin-1 showed a greater increase in the denervated muscles from dexamethasone-treated rats than in those from saline-treated ones. The simplest interpretation of these findings is that the steroid treatment promotes the activation of atrogin-1/MAFbx gene. This is compatible with a recent report that the upregulation of atrogin-1 mRNA was inhibited in muscles of sepsis rats treated with a glucocorticoid inhibitor (RU 38486) [21]. Therefore, there is a possibility that the upregulation of atrogin-1/MAFbx may enhance the ubiquitin-proteasome proteolytic pathway, and then induce MHC I loss in denervated soleus muscle from dexamethasone-treated rats.

Previous studies provided an evidence of increases in proteasome subunits, including the RC3 and ubiquitin genes, in denervated or dexamethasone-treated muscles [32, 33, 39]. In our study, however, on day 2 the mRNA encoding RC3 tended to increase in the denervated muscles of both types of experimental rats relative to the control muscles, but the values did not reach significance. This suggests that RC3 mRNA levels increase immediately after denervation and/or dexamethasone treatment but that changes in the gene may be small in comparison to those in ubiquitin-ligase atrogin-1. Furthermore, the differences in the results of previous reports and our study may be due to differences in the animal species or analytical procedure used.

In summary, we found the downregulation of MHC I mRNA and upregulation of atrogin-1 mRNA in the denervated muscles of dexamethasone-treated rats established as an animal model of CIM. The downregulation of the MHC I gene suggests that a decreased myosin transcription rate or decreased myosin mRNA stability in part functions in myosin loss. The upregulation of atrogin-1 gene speculates that multiple proteins including myosin may be degraded by an accelerated ubiquitin-proteasome system in skeletal muscles of this myopathy. Additional studies using inhibitors of the ubiquitin-proteasome pathway, for example, would be necessary to clarify the pathomechanism of this myopathy.

Acknowledgements

We are grateful to Dr. T. Ito and Dr. S. Fujimoto for their technical advice, as well as to Mrs. M. Ono and Mrs. K. Hirano for their technical assistance.

References

1 Gutmann L, Gutmann L: Critical illness neuropathy and myopathy. Arch Neurol 1999;56:527–528.

2 MacFarlane IA, Rosenthal FD: Severe myopathy after status asthmaticus. Lancet 1977;ii:615.

3 Al-Lozi MT, Pestronk A, Yee WC, Flaris N, Cooper J: Rapidly evolving myopathy with myosin-deficient muscle fibers. Ann Neurol 1994;35:273–279.

4 Danon MJ, Carpenter S: Myopathy with thick filament (myosin) loss following prolonged paralysis with vecuronium during steroid treatment. Muscle Nerve 1991;14:1131–1139.

5 Deconinck N, Van Parijs V, Beckers-Bleukx G, Van den Bergh P: Critical illness myopathy unrelated to corticosteroids or neuromuscular blocking agents. Neuromusc Disord 1998;8:186–192.

6 Helliwell TR, Wilkinson A, Griffithst RD, McClelland P, Palmer TEA, Bone JM: Muscle fibre atrophy in critically ill patients is associated with the loss of myosin filaments and the presence of lysosomal enzymes and ubiquitin. Neuropathol Appl Neurol 1998;24:507–517.

7 Hirano M, Ott BR, Raps EC, Minetti C, Lennihan L, Libbey NP, Bonilla E, Hays AP: Acute quadriplegic myopathy: A complication of treatment with steroids, nondepolarizing blocking agents, or both. Neurology 1992;42:2082–2087.

8 Lacomis D, Giuliani MJ, Van Cott A, Kramer DJ: Acute myopathy of intensive care: Clinical, electromyographic, and pathological aspects. Ann Neurol 1996;40:645–654.

9 Larsson L, Li X, Edstrom L, Eriksson LI, Zackrisson H, Argentini C, Schiaffino S: Acute quadriplegia and loss of muscle myosin in patients treated with nondepolarizing neuromuscular blocking agents and corticosteroids: Mechanisms at the cellular and molecular levels. Crit Care Med 2000;28:34–45.

10 Minetti C, Hirano M, Morreale G, Pedemonte M, Cordone G, Hays AP, Bonilla E: Ubiquitin expression in acute steroid myopathy with loss of myosin filaments. Muscle Nerve 1996;19:94–96.

11 Massa R, Carpenter S, Holland P, Karpati G: Loss and renewal of thick myofilaments in glucocorticoid-treated rat soleus after denervation and reinnervation. Muscle Nerve 1992;15:1290–1298.

12 Rich MM, Pinter MJ, Kraner SD, Barchi RL: Loss of electrical excitability in an animal model of acute quadriplegic myopathy. Ann Neurol 1998;43:171–179.
13 Rouleau G, Karpati G, Carpenter S, Soza M, Prescott S, Holland P: Glucocorticoid excess induces preferential depletion of myosin in denervated skeletal muscle fibers. Muscle Nerve 1987;10:428–438.
14 Hershko A, Ciechanover A: The ubiquitin system. Annu Rev Biochem 1998;67:425–479.
15 Mitch WE, Goldberg AL: Mechanisms of muscle disease: The role of the ubiquitin-proteasome pathway. N Engl J Med 1996;335:1897–1905.
16 Hasselgren PO, Fischer JE: The ubiquitin-proteasome pathway. Review of a novel intracellular mechanism of muscle protein breakdown during sepsis and other catabolic conditions. Ann Surg 1997;225:307–316.
17 Coux O, Tanaka K, Goldberg AL: Structure and functions of the 20S and 26S proteasomes. Annu Rev Biochem 1996;65:801–847.
18 Varshavsky A: The N-end rule pathway of protein degradation. Genes Cells 1997;2:13–28.
19 Gomes MD, Lecker SH, Jagoe RT, Navon A, Goldberg AL: Atrogin-1, a muscle- specific F-box protein highly expressed during muscle atrophy. Proc Natl Acad Sci USA 2001;98:14440–14445.
20 Bodine SC, Latres E, Baumhueter S, Lai VK, Nunez L, Clarke BA, Poueymirou WT, Panaro FJ, Na E, Dharmarajan K, Pan ZQ, Valenzuela DM, DeChiara TM, Stitt TN, Yancopoulos GD, Glass DJ: Identification of ubiquitin ligases required for skeletal muscle atrophy. Science 2001;294:1704–1708.
21 Wray CJ, Mammen JM, Hershko DD, Hasselgren PO: Sepsis upregulates the gene expression of multiple ubiquitin ligases in skeletal muscle. Int J Biochem Cell B 2003;35:698–705.
22 Talmadge RJ, Roy RR: Electrophoretic separation of rat skeletal muscle myosin heavy-chain isoforms. J Appl Physiol 1993;75:2337–2340.
23 Kumamoto T, Ueyama H, Watanabe S, Murakami T, Araki S: Effect of denervation on overdevelopment of chloroquine-induced autophagic vacuoles in skeletal muscles. Muscle Nerve 1993;16:819–826.
24 Laemmli VK: Cleavage and structural proteins during the assembly of the head of bacteriophage T4. Nature 1970;227:680–685.
25 Lowry OH, Roseborough NJ, et al: Protein measurement with the Folin phenol reagent. J Biol Chem 1951;193:265–275.
26 Chomczynski P, Sacchi N: Single-step method of RNA isolation by acid guanidium thiocyanate-phenol-chloroform extraction. Anal Biochem 1987;162:156–159.
27 Tanaka K, Fujiwara T, Kumatori A, Shin S, Yoshimura T, Ichihara A, Tokunaga F, Aruga R, Iwanaga S, Kakizuka A, Nakanishi S: Molecular cloning of cDNA for proteasomes from rat liver: Primary structure of component C3 with a possible tyrosine phosphorylation site. Biochemistry 1990;29:3777–3785.
28 Wright C, Haddad F, Qin AX, Baldwin KM: Analysis of myosin heavy chain mRNA expression by RT-PCR. J Appl Physiol 1997;83:1389–1396.
29 Tso JY, Sun XH, Kao TH, Reece KS, Wu R: Isolation and characterization of rat and human glyceraldehydes-3-phosphate dehydrogenase cDNAs: Genomic complexity and molecular evolution of the gene. Nucleic Acids Res 1985;13:2485–2502.
30 Kinoshita T, Imamura J, Nagai H, Shimotohno K: Quantification of gene expression over a wide range by the polymerase chain reaction. Anal Biochem 1992;206:231–235.
31 Huey KA, Bodine SC: Changes in myosin mRNA and protein expression in denervated rat soleus and tibialis anterior. Eur J Biochem 1998;256:45–50.
32 Medina R, Wing SS, Goldberg AL: Increase in levels of polyubiquitin and protease mRNA in skeletal muscle during starvation and denervation atrophy. Biochem J 1995;307:631–637.
33 Wing SS, Goldberg AL: Glucocorticoids activate the ATP-ubiquitin-dependent proteolytic system in skeletal muscle during fasting. Am J Physiol 1993;264:E668–E676.
34 Fischer D, Sun X, Gang G, Pritts T, Hasselgren PO: The gene expression of ubiquitin ligase E3α is upregulated in skeletal muscle during sepsis in rats: Potential role of glucocorticoids. Biochem Bioph Res Commun 2000;267:504–508.
35 Hobler SC, Wang JJ, Williams AB, Melandri F, Sun X, Fischer JE, Hasselgren PO: Sepsis is associated with increased ubiquitin-conjugating enzyme E214k mRNA in skeletal muscle. Am J Physiol 1999;276:R468–R473.
36 Hobler SC, Williams A, Fischer D, Wang JJ, Sun X, Fischer JE, Monaco JJ, Hasselgren PO: Activity and expression of 20S proteasome are increased in skeletal muscle during sepsis. Am J Physiol 1999;277:R434–R440.
37 Mitch WE, Bailey JL, Wang X, Jurkovitz C, Newby D, Price SR: Evaluation of signals activating ubiquitin-proteasome proteolysis in a model of muscle wasting. Am J Physiol 1999;276:C1132–C1138.
38 Tawa NE Jr, Odessey R, Goldberg AL: Inhibitors of proteasome reduce the accelerated proteolysis in atrophying rat skeletal muscles. J Clin Invest 1997;100:197–203.
39 Wing SS, HAAS AL, Goldberg AL: Increase in ubiquitin-protein conjugates concomitant with the increase in proteolysis in rat skeletal muscle during starvation and atrophy denervation. Biochem J 1995;307:639–645.

Clin Exp Allergy 2005; 35:1214–1219 doi:10.1111/j.1365-2222.2005.02323.x

Cysteinyl leukotrienes induce monocyte chemoattractant protein 1 in human monocytes/macrophages

T. Ichiyama, M. Hasegawa, Y. Ueno, H. Makata, T. Matsubara and S. Furukawa
Department of Pediatrics, Yamaguchi University School of Medicine, Yamaguchi, Japan

Summary

Background Monocytes/macrophages have a cysteinyl leukotriene 1 (CysLT1) receptor, but its function is poorly understood.

Objective To elucidate the biological function of the CysLT1 receptor of human monocytes/macrophages.

Methods We examined the production of TNF-α, IL-1β, IL-2, IL-4, IL-6, IL-8, IL-10, monocyte chemoattractant protein 1 (MCP-1), macrophage colony-stimulating factor (M-CSF), and eotaxin induced by CysLTs (leukotriene (LT)C4, -D4, and -E4) in THP-1 cells, a human monocytic leukaemia cell line, and peripheral blood $CD14^+$ monocytes/macrophages. Moreover, we examined the effect of CysLTs on the expression of β-chemokine receptor 2B (CCR2B) as the receptor of MCP-1 by Western blot analysis.

Results ELISA revealed that CysLTs induced MCP-1 in THP-1 cells and peripheral blood $CD14^+$ monocytes/macrophages, but not other cytokines. PCR demonstrated that CysLTs increased MCP-1 mRNA expression in THP-1 cells, and Western blotting showed that CysLTs increased the expression of CCR2B in THP-1 cells. Moreover, we demonstrated that pranlukast, a CysLT1 receptor antagonist, blocked MCP-1 production by CysLTs in THP-1 cells almost completely, and partially inhibited MCP-1 release by CysLTs in peripheral blood $CD14^+$ monocytes/macrophages and CCR2B expression by CysLTs in THP-1 cells.

Conclusion CysLTs induce MCP-1 and increase CCR2B expression in human monocytes/macrophages.

Keywords CCR2B, cysteinyl leukotrienes, monocyte chemoattractant protein 1, monocytes/macrophages, pranlukast
Submitted 13 October 2004; revised 26 April 2005; accepted 7 July 2005

Introduction

Various roles of cysteinyl leukotrienes (CysLTs), such as leukotriene C4 (LTC4), -D4, and -E4, have been reported in bronchial asthma [1–4]. CysLTs induce contraction of the tracheal muscle [1]. CysLTs have potent effects on leucocyte trafficking, airway mucus secretion, and collagen synthesis [2–4]. Normal peripheral blood leucocytes, such as basophils, eosinophils, B lymphocytes, and monocytes/macrophages, have a CysLT1 receptor [5]. However, the function of these cells, especially monocytes/macrophages, is poorly understood.

Alveolar macrophages (AM) are the most abundant cells not only in the alveoli and distal air spaces but also in the conducting airways [6]. In asthma, AM are activated [7]. Activated AM may participate in the inflammatory events associated with allergic disease of the lower airways, including release of cytokines, chemokines, arachidonic acid metabolites, products of activated O_2, and by direct interaction with T lymphocytes [8–11].

We examined cytokine production, including TNF-α, IL-1β, IL-2, IL-4, IL-6, IL-8, IL-10, monocyte chemoattractant protein 1 (MCP-1), macrophage colony-stimulating factor (M-CSF), and eotaxin, of human monocytes/macrophages induced by CysLTs to elucidate the biological function of the CysLT1 receptor of human monocytes/macrophages.

Correspondence: Takashi Ichiyama, Department of Pediatrics, Yamaguchi University School of Medicine, 1-1-1 Minamikogushi, Ube, Yamaguchi 755-8505, Japan.
E-mail: ichiyama@yamaguchi-u.ac.jp

Methods

Cell culture and stimulation conditions

THP-1 cells [12], a human monocytic leukaemia cell line that has a CysLT1 receptor [13], obtained from the American Type Culture Collection, were maintained at 37 °C under humidified 5% CO_2 as stationary cultures. The cells were grown in RPMI 1640 medium containing 10% FBS, 100 U/mL of penicillin, and 100 μg/mL of streptomycin. Peripheral blood mononuclear cells (PBMC) were obtained from heparinized blood from 10 healthy medication-free volunteers, with informed consent, by Histopaque 1077 (Sigma

Chemical Co., St Louis, MO, USA) gradient centrifugation and washing. Purification of individual cell subpopulations was achieved with a high magnetic gradient Mini MACS purification system (Miltenyi, Sunnyvale, CA, USA). $CD14^+$ monocytes/macrophages were isolated by depletion of non-monocytes (negative selection) with a Monocyte Isolation Kit II (Miltenyi). The purity of the isolated cells was determined using the respective fluorescein isothiocyanate (FITC)-conjugated monoclonal antibodies (Becton-Dickinson Biosciences, San Diego, CA, USA) and flow cytometric analysis (FACScan; Becton-Dickinson Biosciences). Cells were exposed to LTC4, -D4, or -E4 (Sigma Chemical Co). Some samples were pretreated with pranlukast, a CysLT1 receptor antagonist, provided by ONO Pharmaceutical Co. (Osaka, Japan) for 30 min before the addition of CysLTs. Supernatant fluid, both before and after the addition of CysLTs, was harvested for determination of cytokine levels and then stored at −20 °C.

Determination of the concentrations of cytokines

The concentrations of TNF-α, IL-1β, IL-2, IL-4, IL-6, IL-8, and IL-10 in the supernatant fluid were measured with a cytometric bead array (CBA) kit (BD PharMingen, San Diego, CA, USA) according to the manufacturer's instructions, as described previously [14–16], with modification of the data analysis, using GraphPad Prism software (GraphPad Prism Software, San Diego, CA, USA). Briefly, a CBA involves a series of beads exhibiting discrete fluorescence intensities at 670 nm. Each series of beads is coated with a monoclonal antibody against a single cytokine, and a mixture of the beads can detect six cytokines in one sample. A secondary phycoerythrin (PE)-conjugated monoclonal antibody stains the beads proportionately to the amount of bound cytokine. After fluorescence intensity calibration and electronic colour compensation procedures, standard and test samples were analysed with a FACScan flow cytometer equipped with CellQuest software (BD PharMingen). Data were transferred to GraphPad Prism. Starting with standard dilutions, the software performed log transformation of the data and then fitted a curve to 10 discrete points using a four-parameter logistic model. The calibration curve created for each cytokine was used to estimate the cytokine concentrations in the samples. The detection limits for TNF-α, IL-1β, IL-2, IL-4, IL-6, IL-8, and IL-10 were 2.8, 7.2, 2.6, 2.6, 2.5, 3.6, and 2.8 pg/mL, respectively.

The concentrations of MCP-1, M-CSF, and eotaxin in the supernatant fluid were determined with sandwich-type ELISA kits (R&D Systems, Minneapolis, MN, USA). The detection limits for MCP-1, M-CSF, and eotaxin were 5.0, 9.0, and 5.0 pg/mL, respectively.

Reverse transcriptase-polymerase chain reaction

Total RNA was prepared from each cell type using a TRIzol reagent (Invitrogen, Leek, the Netherlands). RT-PCR was performed with Gene Amp and an oligo dT primer (Applied Biosystems, Foster City, CA, USA) for RT, and Taq polymerase (Roche Diagnostics GmbH, Mannheim, Germany) for PCR. The primers used were as follows: (1) MCP-1: forward, 5′-ACTGAAGCTCGCACTCTC-3′, and reverse, 5′-CTTGGGTTGTGGAGTGAG-3′; and (2) GAPDH: forward, 5′-ACCACAGTCCATGCCATCAC-3′, and reverse, 5′-TCCACCACCCTGTTGCTGTA-3′. Quantitation of bands was conducted with a Kodak Digital Science 1D (Eastman Kodak Company, New Haven, CT, USA).

Western blot analysis

Total cell lysates were obtained by the incubation of cell samples in ice-cold lysis buffer (1 mM ethylene diamine tetraacetic acid, 0.2 mM phenylmethylsulphonyl fluoride) with protease inhibitors (1 μM leupeptin and 1 μM pepstatin) and centrifugation to remove debris (12 000 *g* for 10 min at 4 °C). The protein concentrations of the samples were determined with a Bio-Rad (Hercules, CA, USA) protein concentration reagent. Samples containing 20 μg of protein were separated in denaturing 10% polyacrylamide gels and then transferred to polyvinylidene difluoride membranes. After three washes in TBST (40 mM Tris-HCl, pH 7.6, 300 mM NaCl and 0.5% Tween-20), the membranes were incubated with a 1 : 1000 dilution of goat polyclonal anti-β-chemokine receptor 2B (CCR2B) antibodies (Santa Cruz Biotechnology, Santa Cruz, CA, USA) in TBST containing 5% non-fat dry milk at room temperature for 1 h. After three washes in TBST, the membranes were incubated with a 1 : 2500 dilution of horseradish peroxidase-conjugated rabbit anti-goat IgG (Bio-Rad) for 1 h at room temperature. Immunoreactive proteins were detected using enhanced chemiluminescence (Amersham, Arlington Heights, IL, USA) and analysed by radiography. Quantification of bands was conducted with a Kodak Digital Science 1D.

Statistical analysis

The values of cytokine concentrations are expressed as means ± SD. Statistical analysis was performed with the Wilcoxon's matched paired test, with a *P*-value of less than 0.05 being taken as significant.

Results

Figure 1 demonstrates MCP-1 release by the stimulation of LTC4, -D4, and -E4 for 4 h in THP-1 cells. CysLTs (10^{-6}–10^{-8} M) induced MCP-1 in THP-1 cells, and LTC4 and -D4 significantly induced MCP-1 more than -E4 ($P<0.01$). Interestingly, 10^{-7} M of LTC4 and -D4 significantly induced MCP-1 more than 10^{-6} and 10^{-8} M of those, respectively ($P<0.01$). CysLTs (10^{-6} to 10^{-8} M) did not induce TNF-α, IL-1β, IL-2, IL-4, IL-6, IL-8, IL-10, M-CSF, or eotaxin in THP-1 cells (Table 1). The time course of MCP-1 production was examined by incubating THP-1 cells with 10^{-6} to 10^{-8} M LTD4 during a 24 h period (Fig. 2). MCP-1 production could be observed 1 h after the addition of LTD4, and gradually increased over 24 h.

The concentrations of MCP-1 in the culture fluid of THP-1 cells exposed to CysLTs, in the presence or absence of pranlukast, for 4 h are shown in Fig. 3. The production of MCP-1 induced by CysLTs was significantly inhibited by 10^{-6}–10^{-8} M pranlukast. The effect of pranlukast was dose related. The time courses of the inhibitory effects of

